No. 88 – June 1997

TELESCOPES AND INSTRUMENTATION

The M1 Cell - M3 Tower Undergoes Tests in Europe

S. STANGHELLINI, M. HESS, G. RAFFI, J.-M. MORESMAU, F. KOCH, M. KRAUS, ESO

The M1 cell - M3 tower of the Very Large Telescope is undergoing final integration and testing at the GIAT factory in St. Chamond. There, at the same factory (previously Creusot Loire) where the 3.6-m telescope of ESO was built twenty years ago, the French consortium of GIAT Industries and SFIM Industries, selected by ESO for the design and construction of the M1 cell - M3 tower, is working to complete the European testing of the first unit of the M1 cell-M3 tower.

The most noticeable part of the system, the laser welded, white painted primary mirror cell, whose construction was finished in summer last year, is now fully equipped with the 150 axial supports and the 72 lateral supports of the primary mirror. Steel pipes of various diameters, all filled under vacuum with oil, interconnect the hydraulic pads to form the whiffle-tree networks supporting in the most accurate way the weight of the primary mirror. The force actuators, used for active optics correction are mounted and linked to the Local Control Unit through their dedicated bus. Hundreds of metres of cable connect the many electrical boxes, the sensors and the other equipment spread inside the cell. Although not much space has been left free, still remarkable is the accessibility provided by the cell design. On the top surface of the cell, the axial interfaces to the mirror with their tiny flexures are now in position, optically adjusted to within a few tenths of a millimetre. The M3 tower rotation mechanics, embedded in the centre of the cell, is fully operational. Only missing at the time of writing is the cold plate used to cool down the mirror to eliminate or reduce mirror seeing. The plate, located just below the primary mirror, will be mounted only at the end of the testing phase to allow at any

Figure 1: First integration of the M1 dummy mirror in the cell.

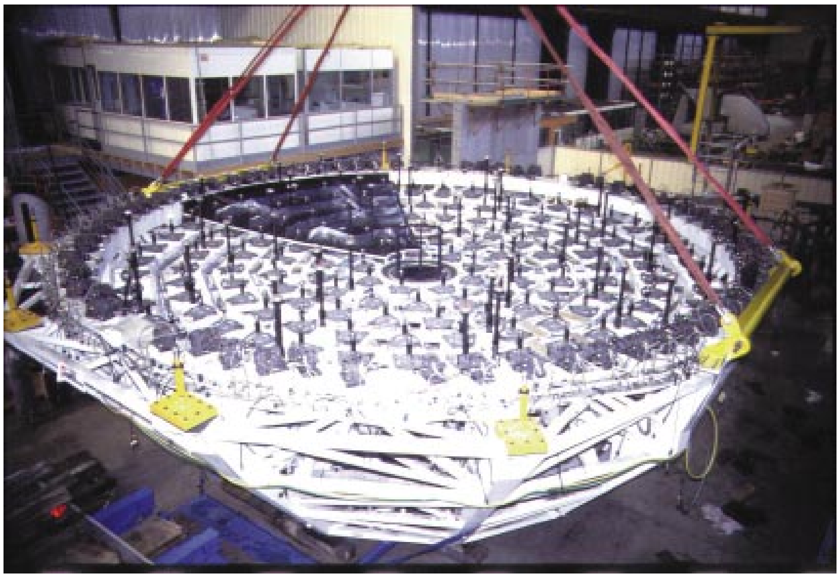

Figure 2: Top view of the fully equipped M1 cell. Also visible is one sector of the cold plate.

Figure 3: The M1 cell is brought below the M1 dummy hanging in the handling tool to test the integration procedure.

time visual control of the mirror axial interfaces.

The testing activities in Europe started in February with the hardware and software tests of the LCU. Afterwards, the active supports were tested. The M3 tower upper part was then installed on the rotation stage, aligned and tested.

One remarkable phase was the introduction of the primary mirror dummy. This operation was accomplished with the help of special jigs which allowed the mirror to be kept centred while it was slowly lowered on the tiny axial interface devices by means of the handling supports located in the cell. Once the mirror was integrated, it has been possible to test and tune the mirror position control system, allowing the adjustment of the mirror in five degrees of freedom.

At the time of writing, one important milestone in the project has been achieved with the joint testing of the M1 cell with the huge handling tool, which will later be installed in the Mirror Maintenance Building in Chile. This machine, whose specification and preliminary design were prepared by Max Kraus of ESO, allows the removal of the four primary mirrors from the transport container and their rapid and safe transfer between the M1 cells and the coating plant. The MMB Handling Tool, in its final version designed and built by GIAT, was erected in the St. Chamond assembly hall, near the M1 cell, to prove its complete functionality and to check the interfaces. The testing included, among other things, a complete transfer cycle of the primary mirror dummy from the transport container into the M1 cell and back into the container. The European testing of the handling tool is now finished – the tool is being dismantled and packed in containers to be shipped to Paranal.

The final and most exciting step of the testing phase is the tests in the inclined test set-up. To reproduce operating conditions similar to those of the telescope, a large and stiff steel frame simulating the telescope centrepiece has been manufactured. The frame is mounted by means of bearings on top of two concrete columns, built in the assembly hall. The M1 cell with the primary mirror and the M3 tower will then be attached to this structure at its twelve interface flanges and gradually rotated up to 90 degrees. This will provide the possibility of the complete verification of the system against the technical specification.

The successful completion of this test, scheduled for the end of July 1997, will allow GIAT and SFIM to ship the M1 cell to Chile. In the mean time the handling tool will have been erected, in time for the final joint acceptance testing of both the handling tool and the M1 cell-M3 tower.

S. Stanghellini
sstanghe@eso.org

Figure 4: The M1 cell and M1 dummy is lifted by the handling tool.

The Secondary Unit of the VLT Approaches Delivery

S. STANGHELLINI, G. JANDER, A. MICHEL, A. VAN KESTEREN, M. DUCHATEAU, W. ANSORGE, ESO

There has been significant progress in the manufacture of the first secondary mirror unit of the VLT since the last report in *The Messenger* (No. 86, December 1996). During the first months of 1997, tests of the various subassemblies (focusing, centring, chopping and sky-baffle mechanisms) were completed and final integration was achieved in the clean assembly room of Dornier Satellitensysteme in Friedrichshafen, Germany. The systematic tests performed prior to final integration, including tests of the electronics and software integration tests were helpful for early detection and elimination of error sources affecting performance of the M2 Unit.

Before the end of April 1997 the Mandatory Inspection Point meeting which was held between Dornier and ESO, as foreseen in the contract, formally concluded the manufacturing and integration activities and opened the acceptance test phase, structured in four distinct steps. The first step is related to Electromagnetic Compatibility. The second step is the testing of the software. The third step checks in depth the kinematic and the thermal performance of the unit, taking also into account the environmental conditions foreseen on site. The final step is constituted by the dynamic and stability testing.

As per today the Electromechanical Unit has undergone the Electromagnetic Compatibility test and the Software tests. The electromagnetic compatibility tests, which were performed in the anechoic chamber of Dornier (see Fig. 1), showed the ability of the unit to perform properly in the electromagnetic environment expected in the telescope. Similarly good results were also obtained during the software tests.

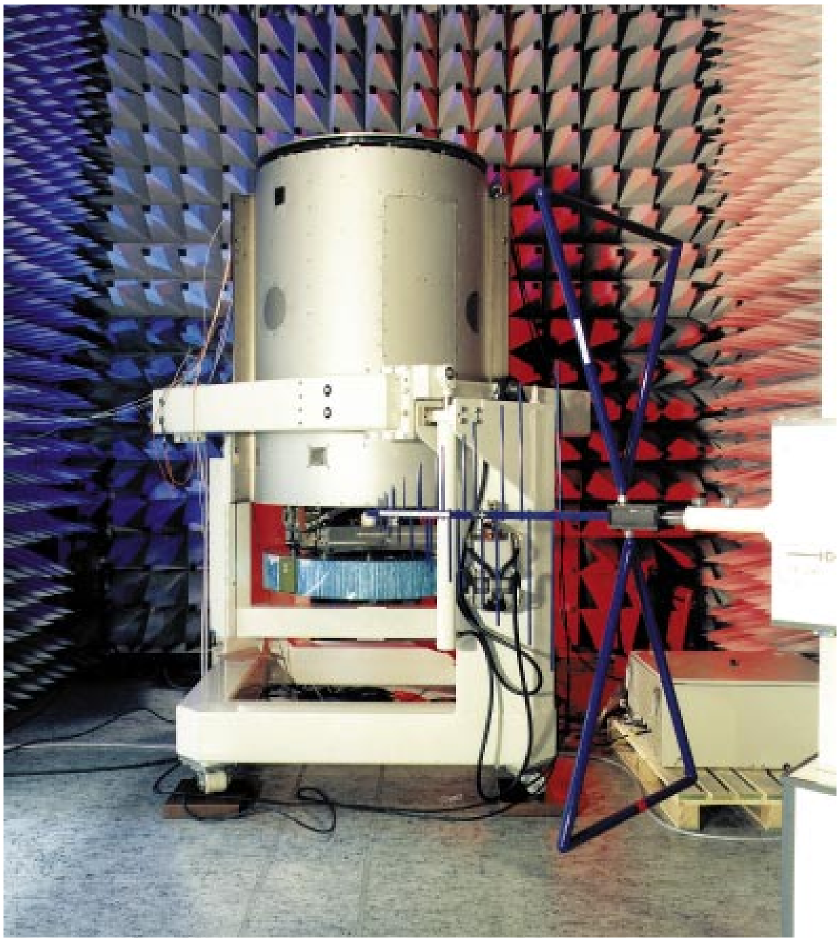

Figure 1: The M2 Unit equipped with the M2 dummy in the anechoic chamber of Dornier. (Photo Dornier).

At the time of writing, the kinematic and thermal tests have started. The tests shall demonstrate the ability of the M2 Unit to position the secondary mirror along the five controlled degrees of freedom with the required accuracy. These tests are performed with a dummy secondary mirror. Some of the kinematic performances have been already demonstrated at ambient temperature. The M2 Unit is now being cooled and maintained at a temperature near 0° C while the kinematic functions are operated. During the thermal tests the temperature of both critical internal parts and the external skin is monitored.

Figure 2: The Beryllium secondary mirror during polishing at REOSC Optique.

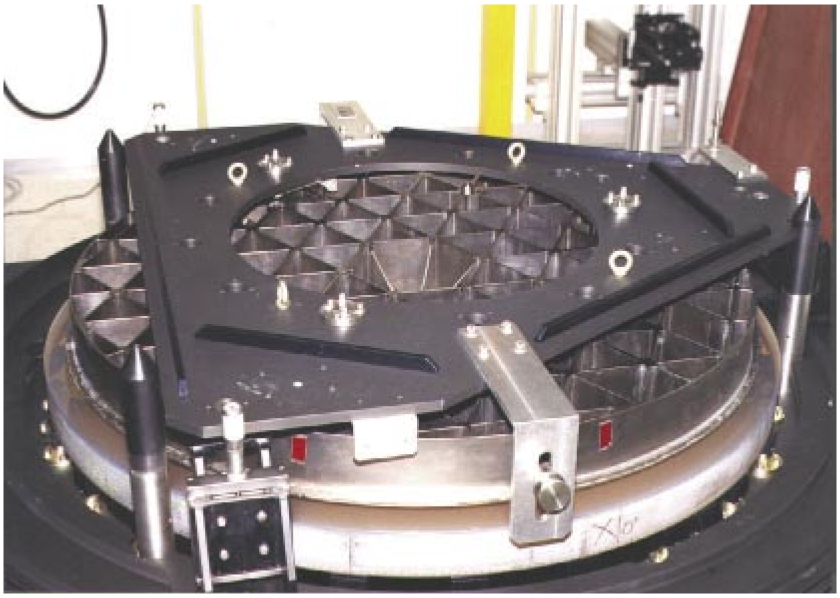

Figure 3: The secondary mirror mounted in the optical test set-up. Below the mirror the Zerodur matrix used for optical testing is visible.

In the meantime, polishing of the first of the four Beryllium secondaries at REOSC Optique in Paris is well progressing. The final polishing is almost completed with the optical quality approaching the specified Central Intensity Ratio. During the polishing, intermediate testing was done by means of a matrix test set-up (see Figs. 2 and 3), after integration of the mirror in its final Titanium cell. At carefully chosen intervals during the polishing, the mirror was submitted to thermal cycling to reduce internal stress and obtain a long-term optical stability. The remaining tasks ahead are related to the cutting of the external edge of the mirror, necessary because in its final dimensions the secondary is undersized and defines the pupil of the telescope. After the cutting, the optical figure will be verified to see if a final polishing retouch is necessary. These activities are expected to be completed during the summer.

Subsequently, the mirror will be shipped to Dornier where it will be integrated into the electromechanical unit. At this point, the fourth and last step of the M2 Unit tests will start in a set-up simulating the telescope spider. The purpose is to verify that there is no structural interaction between the M2 Unit and the telescope structure since this could lead to reduced chopping performance. The M2 Unit is expected to be delivered in late summer in time for the integration in the telescope on Cerro Paranal.

S. Stanghellini
sstanghe@eso.org

The VLT Mirror Coating Unit Ready for Shipment

M. SCHNEERMANN and M. GROESSL, ESO

In August 1995, the European Southern Observatory signed a contract with Linde AG, Germany, for the supply of the coating unit for the VLT mirrors. Together with their main subcontractors, BOC Coating Technology, UK, and Deggendorfer Werft, Germany, Linde meanwhile completed the development, construction and pre-commissioning of the coating unit in Deggendorf. On the 14th of May 1997, the preliminary acceptance review meeting took place, and it was concluded that the coating unit is fully capable of producing aluminium coating on the VLT mirrors with the specified quality.

The coating unit (see pictures of the coating unit inside the facilities of Deggendorfer Werft, located directly at the Danube river) is a large vacuum chamber with a diameter of 9.4 metres and a volume of about 122 m^3. The high vacuum is generated by 8 cryo-pumps which are located on top of the vacuum chamber. The chamber is divided into two halves by a horizontal flange sealed by O-rings (see Fig. 2). The mirror is loaded into the lower half of the chamber onto a whiffle-tree support system with

Figure 1: The coating unit for the VLT mirror substrates at Deggendorfer Werft premises. The circular platform on top of the chamber provides personal access to the cryo-pumps, feedthrough, vacuum gauges, etc. located on top of the chamber.

Figure 2: The lower part of the coating unit vacuum chamber moved out beneath the fixed upper part. Inside the chamber the rotatable whiffle-tree for support of the primary mirror is visible. Here, a steel plate serves as a dummy mirror for testing purposes.

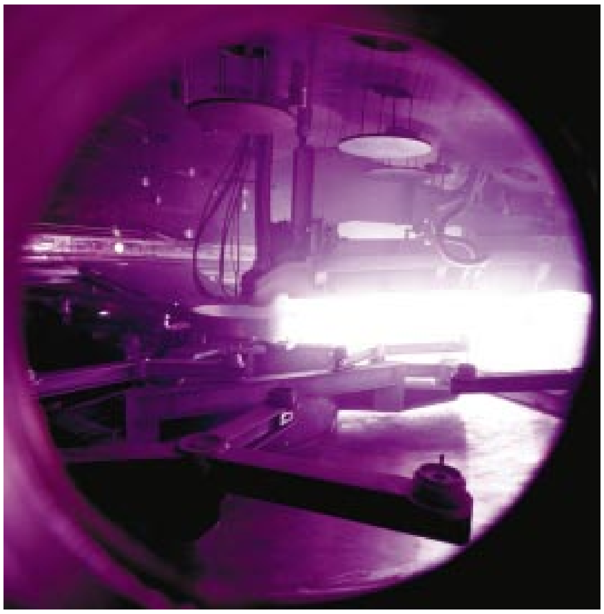

Figure 3: A view through one of the vacuum chamber windows while the glow discharge cleaning device is fired. The blue light is emitted from the plasma generated by the glow discharge electrodes. Above the shiny discharge area the contours of the sputter source arrangement are visible. In the lower part of the picture one recognises the whiffle-tree loaded with the dummy.

27 axial pads and laterally secured inside the central hole by 6 pads. This support system is fixed on a central shaft which is driven by a high-precision motor gear system arranged below the vacuum chamber. The 80 nanometre (i.e. 80 millionth of a millimetre) thin aluminium coating is deposited by utilising magnetron sputtering technology. During the coating process, the mirror is rotated slowly under the sputter source, which is fixed inside the upper half of the vacuum chamber. The lower half of the vacuum chamber is mounted onto an air cushion vehicle via 4 large spindles for closing and opening of the vacuum chamber. For loading and unloading of the mirrors, the lower half of the chamber is moved on 8 air-cushions from the coating unit location to the mirror handling tool and vice versa.

During the next weeks, the coating unit is dismantled at Deggendorfer Werft, packed and loaded onto a river barge. The vacuum chamber with its 9.4 metre diameter and 60 tons overall weight will be one of the largest pieces shipped for the VLT project. The transport goes from Deggendorf on the Danube, Main and Rhine rivers to Antwerp in Belgium. There the coating unit is loaded onto the ship to Antofagasta leaving beginning of June. The coating unit will finally arrive on Paranal by the end of July, 1997. There it will be installed inside the mirror maintenance building. The completion of the erection and provisional acceptance of the coating unit is planned for the end of October 1997.

M. Schneermann
mschneer@eso.org

Figure 4: The 'giant dome' – The upper vacuum chamber part carrying the sputter source arrangement (top right) and the catcher disks below the cryo-pumps (top centre). The lower chamber part is transported out by means of the air cushion cart (orange) moving along the metallic strips (bottom left and right).

New Cryostats for Scientific CCD Systems in the VLT Era

J.-L. LIZON, ESO

Introduction

Since the installation of the first device on La Silla in 1982, the CCD has become the standard detector in ESO's optical instruments. In order to use a CCD for astronomy, it must be cooled to 140–160 deg K to reduce dark current to a negligible level. For this reason, the CCD detectors are mounted in vacuum dewars with cooling provided by liquid nitrogen (77 deg K). In addition to keeping the CCD cold, the dewar also serves the very important purpose of holding the CCD in a very rigid position, with motion of less than 3 microns as the telescope points to different positions in the sky.

During the past 15 years, ESO has installed 36 different CCDs at the telescopes on La Silla, of which 10 are presently operational. For these CCDs, two generations of CCD dewars have been used. Most of the CCDs are cooled using the well-known HD-2(8) dewar made by InfraRed Laboratory.

CCD technology has developed very rapidly during the last few years so that the size of currently available chips is much larger than the preceding generations and it is not possible to fit the new large devices into the old dewars. Besides having enough room to house the CCD, more cooling "power" is needed for larger CCDs. In a well-constructed dewar, the most important heat load is the thermal radiation of the window. With a larger window, the old HD-2(8) dewar would need refilling twice a day to keep the detector cold.

Figure 1 : Continuous-flow cryostat.

Since ESO has a need for a large number of optical detector systems during the VLT era, now is the opportune time to reconsider the complete re-design of the CCD dewars.

Requirements

A major goal of the VLT plan is the operation of the Paranal facility with the minimum number of staff. Since the filling of dewars with liquid nitrogen can be a labour-intensive process, one goal of a new design must be the maximisation of the nitrogen "hold time". After investigation of the cooling requirements of each instrument, it was clear that a universal system cannot be designed for all instruments. However, we have been able to reduce the complexity by splitting the dewar functionality into two parts:

- a detector head that holds the CCD detectors and associated electronics, such as wiring, analogue filters, preamplifier and temperature sensing and control,
- a cryostat that provides the cooling function.

To our knowledge, the new ESO design is one of the few that distinctly splits the dewar into these two parts. By doing this, we have been able to design a single detector head that can be used for nearly all of the instruments. The interface between the cryostat and the head has been designed such that an exchange of cryostat is a very simple operation which does not require any special adjustment. Apart from the time due to the vacuum and cryogenic operation (warming-up, evacuation, cooling) an exchange of cryostat does not require more than a few minutes.

The major differences in various instruments are related to the cryostat function and we have designed a system optimised for each of the two major categories: static instruments and movable instruments.

Static Instruments – Continuous Flow Cryostat

Some large instruments or instruments fitted with optical fibres are simply resting on the Nasmyth platform and do not move relative to the telescope building. UVES is the first instrument of this type and, being a high-resolution spectrograph, it is very sensitive to any type of disturbance, especially thermal variations. For this reason the complete instrument, including the two detector systems, is surrounded by a thermal enclosure. It would be a major source of

Figure 2 : Bath cryostat, Cassegrain version.

disturbance if it were necessary to open the thermal enclosure to refill the detector cryostats every day. Therefore, for UVES, and other Nasmyth and coudé instruments, we have developed a continuous-flow cryostat. This cryostat is based on a continuous circulation of coolant supplied from a de-localised reserve of liquid nitrogen. This system uses a large tank of liquid nitrogen so that the cooling operates autonomously for relatively long periods between replacement of the nitrogen reservoir. Another advantage of the continuous-flow cryostat is that it only occupies a small volume at the instrument. Figure 1 shows the compactness of the continuous-flow cryostat relative to the detector head.

One prototype cryostat based on this principle has been successfully operating at the CES since March 1995. Based on this experience, we modified the design to make a more compact cryostat which has achieved an especially low rate of nitrogen consumption. Using a 120-litre storage tank, the standard selected for the VLT, the hold time can easily reach 1 month.

Movable Instruments – Bath Cryostat

These instruments are directly bolted onto the telescope adapter-rotator and thus move with the telescope. For these instruments, the nitrogen must be stored in a cryostat tank that is attached directly to the detector head. This type is called a “bath cryostat”, since the coolant is stored in a local tank (i.e. “bath”) of liquid nitrogen. The design goals for the bath cryostat include: (a) hold time of at least 2 days, and (b) an interface similar to the old HD-2(8) dewar which offers the possibility of upgrades of systems in operation on La Silla.

Many users of bath cryostat dewars are aware of the constraint that only 50% of the tank can be filled, otherwise the liquid nitrogen can be dumped out of the tank when the telescope is moved. A tank only half full will provide only half of the hold time of a full tank. A major new feature of the new ESO bath cryostat design is a special anti-overflow device that allows 90% filling of the nitrogen tank, independent of the angular position of the cryostat. This can be achieved if the motion of the cryostat axis is limited to half a sphere (relative to the gravity vector), which is true for the two instrument adapters of the VLT (azimuth-elevation telescope mount).

The design of the bath cryostat was a compromise between the total container mass and the mass of the liquid nitrogen in the tank. Our goal was to maximise the amount of liquid nitrogen in the tank while keeping the outside of the cryostat the same size as the older HD-2(8) design. The new cryostat can be filled to 6 litres, three times the 2 litre capacity of the HD-2(8) design (50% fill).

Two different bath cryostats are needed to accommodate the different motions at the Nasmyth and Cassegrain foci. Figures 2 and 3 respectively show the Cassegrain and the Nasmyth versions of the bath cryostat with the detector head integrated.

Five bath cryostats have been fabricated, assembled and tested. The tests of the cryostat for the first instrument to be equipped with this new system (FORS) have proven that we meet the requirements. Hold time of more than 48 hours has been achieved for a complete system with CCD and temperature control. An agreement based on a technology transfer has been signed with the French company SNLS which is prepared to commercialise this cryostat design.

Acknowledgements

A large part of the success of these various projects is to be attributed to the very patient work of Armin Silber. This development would not have been possible without the full support and confidence of the complete optical detector group first headed by S. D’Odorico and now by J. Beletic.

J.-L. Lizon
jlizon@eso.org

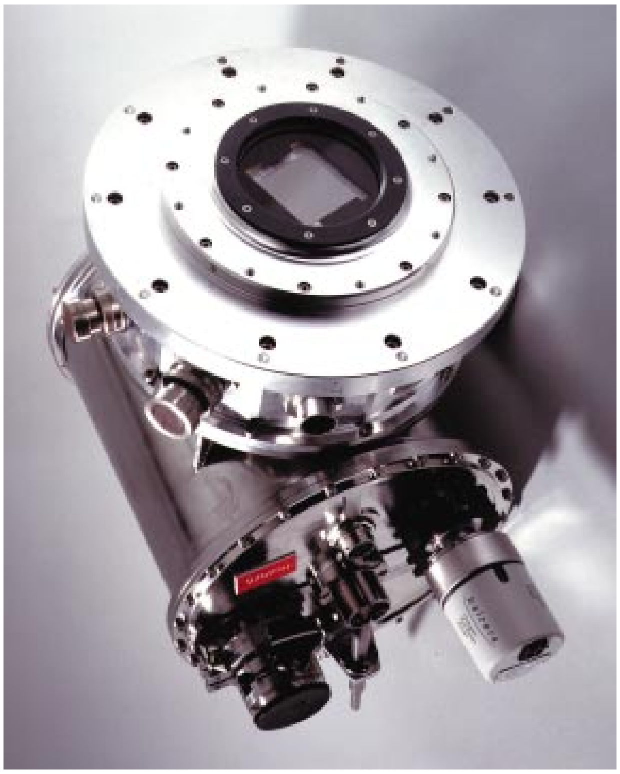

Figure 3 : Bath cryostat, Nasmyth version.

Ground-Based Astronomy in the 10 and 20 μm Atmospheric Windows at ESO: Two New Instruments, VISIR for the VLT and TIMMI2 for La Silla Now Under Way

H.U. KÄUFL, ESO

1. Introduction

This article gives a brief report about the status of ESO's instrument projects for the 10 and 20 μm atmospheric windows. Both projects have passed recently important milestones (contract signature, kick-off meeting) and for both projects the most pressing concern – the availabilty of suitable detector arrays – seems to be no longer of relevance as two manufacturers (SBRC and Rockwell) now offer suitable arrays.

On the other hand, the success of ISO, the European Infrared Space Observatory, may lead to a large increase of requests for ground-based follow-up observations exceeding the capabilities of TIMMI, ESO's present instrument for this kind of astronomy at the 3.6-m telescope.[1] The scientific interest and potential for astronomy in this wavelength range has been described previously in this journal (Käufl, 1993). An exhaustive collection of scientific projects for these instruments, especially VISIR, can be found in the proceedings of the ESO workshop "Science with the VLT"[2].

2. VISIR

The project was prepared by an extensive Phase-A study by a consortium of institutes led by the *Service d'Astrophysique* (SAP-DAPNIA) of the CEA, Saclay (France). The contract between ESO and the consortium led by the *Service d'Astrophysique* was signed on November 7, 1996. Partner to the consortium are the Netherland's Foundation for Research in Astronomy, Dwingeloo (The Netherlands) and the *Institut d'Astrophysique Spatiale*, Orsay (France). The principle investigator for VISIR is Pierre-Olivier Lagage (SAP), the co-investigator is Jan-Willem Pel, Kapteyn Astronomical Institute, Groningen (The Netherlands). VISIR stands for VLT-Imager and Spectrometer for the Mid-Infrared. The result of the phase-A study has been reported recently by the study team in *The Messenger* (Lagage et al., 1995). This article gives both a description of the observing modes (diffraction-limited imaging with variable magnification in the 10 and 20 μm atmospheric windows and low-, medium- and high-resolution spectroscopy (i.e. $\lambda/\Delta\lambda$ approaching 30,000) and the principles of the optomechanics. Thereafter the concept has been subject to a consolidation phase, and for the present status the reader is invited to consult the ESO web-page for VISIR (http://www.eso.org/vlt/instruments/visir/) or the web-page of the consortium (http://www-dapnia.cea.fr/Phys/Sap/Experiences/VISIR/Home_VISIR.html).

At present, VISIR is in its predesign phase where also all relevant prototype tests are being made. Commissioning of VISIR, which shall be mounted to the Cassegrain focus of VLT unit telescope #3, is planned for the first quarter of 2001 and release to visiting astronomers will occur in the third quarter of that year. At the end it should be noted that VISIR is by far the most powerful instrument for this wavelength range under construction for any large telescope project. Moreover VISIR observers will particularly benefit from the VLT site, especially the rather low water vapour content on Paranal.

3. TIMMI2

In the context of the La Silla 2000 initiative of the STC, ESO received a proposal by the Sternwarte Jena (Germany) to replace the present TIMMI instrument

Figure 1: This figure (courtesy University of Jena) shows the optomechanical setup of TIMMI2. The approximate size of this optomechanical assembly is in all directions less than typically 400 mm. The light is entering from the right and after deflection on the collimator mirror sent by a folding mirror through the pupil stop, filter/grism wheel and the objective wheel down towards the detector, a 256 × 256 pixel Rockwell Si:AS BIB detector. The detector – as well as the entire instrument – will be cooled by a commercial 2-stage closed-cycle cooler. The cryostat entrance window is partially obscured by the mask/slit wheel and the retractable λ/2-plate which will be used for polarimetry.

[1]TIMMI is to the best of my knowledge still the only instrument available worldwide for unconditional observations by visiting astronomers. While TIMMI – due to the rapid technical progress in the field – is no longer unique but has formidable competition by various visiting instruments available in the community, its performance has recently been improved thanks to the refurbishment of the 3.6-m telescope in the infrared configuration which will be reported in one of the upcoming issues of *The Messenger.*

[2]*ESO Astrophysics Symposia,* Springer 1995, ed. J.R. Walsh & I.J. Danziger.

at the 3.6-m telescope by an improved version taking advantage of the progress in detector technology. Recently, a corresponding Memorandum of Understanding has been signed by the Sternwarte Jena and ESO. Similar to TIMMI, this new instrument will follow the concept of an 'infrared EFOSC', i.e. it is a focal reducer with variable magnification allowing for grism spectroscopy and polarimetry. The principal investigator for TIMMI2 is Hans-Georg Reimann, Jena (Germany). The TIMMI2 observing modes will be:

- diffraction-limited imaging at 10 and 20 μm
- imaging polarimetry at 10 μm
- low-resolution (i.e. $\lambda/\Delta\lambda$ 200) long-slit spectroscopy at 10 and 20 μm
- a medium-resolution (i.e. $\lambda/\Delta\lambda$ 1000) cross-dispersed Echelle mode is being considered.

For more details please consult the ESO web-page (http://www.eso.org/vlt/instruments/visir/timmi2, or the Sternwarte Jena web-page (http://www.astro.uni-jena.de/Users/rei/timmi2.html. Design work for TIMMI2 has already progressed substantially before the official signature of the Memorandum of Understanding. The present planning for TIMMI2 foresees the release of TIMMI2 to ESO visiting astronomers at the end of 1998. As a concluding remark it should be noted that TIMMI2 will be by far the most advanced instrument available at any observatory (including visiting instruments).

4. Performances

Both VISIR and TIMMI2 will allow for imaging and long-slit spectroscopy with diffraction-limited spatial resolution, i.e. factors of 10 to 20 better than ISOCAM, the imaging instrument of ISO, however, generally at the price of compromised sensitivity. Readers interested in the full details should consult the web pages giving sensitivity estimates for spectroscopy for the different cases. It should be noted that these sensitivity numbers depend largely on the Earth's atmosphere. Within the clear parts of the atmosphere, TIMMI2 and even more VISIR in spectrospcopy are extremely competitive with ISO. In the case of objects smaller than typically 3 arcsec, TIMMI2 and VISIR can outperform ISO substantially. In imaging the point-source sensitivity at 10 μm (10σ in 1 hour) is estimated to be 5 mJy for TIMMI2 and 0.6 mJy for VISIR.

References

H.U. Käufl, 1993, *The Messenger* **72**, p. 42.
P.O. Lagage et al., 1995, *The Messenger* **80**, p. 13.

H.U. Käufl
hukaufl@eso.org

10- and 20-μm Imaging with MANIAC[1]

T. LEHMANN[1], T. BÖKER[2, 3], A. KRABBE[2], J.W.V. STOREY[4]

[1] Astrophysikalisches Institut und Universitäts-Sternwarte Jena, Germany
[2] Max-Planck-Institut für Extraterrestrische Physik, Garching, Germany
[3] Space Telescope Science Institute, Baltimore, USA
[4] School of Physics, University of New South Wales, Sydney, Australia

Introduction

MANIAC is the new Mid- And Near-Infrared Array Camera built at the Max-Planck-Institut für Extraterrestrische Physik (MPE). It is designed as a modular two-channel instrument that will offer simultaneous observations in the near infrared (NIR) from 1 to 5 μm and in the mid-infrared (MIR) from 8 to 28 μm as well as a mid-infrared imaging spectroscopy mode. The first phase of the project, the MIR channel, has been completed and successfully commissioned in March 1996 at the ESO 2.2-m telescope at La Silla. Further improvement of data quality was achieved on a second observing run during October/November 1996 at the same place. In this article we present first results of broad-band N (8–13 μm) and Q (18–23 μm) observations, the latter being the first full Q-band images taken from La Silla.

Mid-Infrared Channel

The MIR channel is based on a 128 × 128 pixel Si:As array manufactured by Rockwell International, U.S.A. The array can be operated in different read-out modes with single read or double sampling being the modes most commonly used. The control electronics from Wallace Instruments, U.S.A., can read out the detector using four output channels at a top speed of 400 images per second.

MANIAC's field of view is 44 × 44 arcsec^2 (scale = 0.345 arcsec/pix) at the Cassegrain focus of the 2.2-m telescope with the f/35 secondary. The spatial resolution is determined by the diffraction limit of the telescope. The camera optics is a purely reflective gold-coated three-mirror system with achromatic performance. At present, the camera is equipped with a total of 13 broad- and narrow-band filters with a spectral resolution between 2 and 70. The filter set is complemented by a circular variable filter (CVF) operating from 7 to 14 μm at a spectral resolution of about 50.

Observations at MIR wavelengths require cryogenic temperatures for the instrument to minimise its own thermal emission. Therefore, detector, filters and mirrors are cooled down to 4.2 K using liquid helium. Technical details about optical design and data-acquisition system are described elsewhere (Böker, 1996, Böker et al., 1997).

Performance

Extensive testing was done in the laboratory and under observing conditions. The detector is linear up to $8 \cdot 10^6$ electrons (full well capacity). The total transmission at 10 μm including optics, filters, and detector is 11%. The measured noise equivalent power in the N-band is NEP = 2. . .5 mJy/arcsec^2 (1σ, 1 hour), depending on the observing conditions we have had during our two runs. Our data show only a small amount of excess noise indicating that the instrument is running close to background-limited performance.

The use of the Q-band filter (18–23 μm) is restricted to good observing conditions, which means a dry atmosphere. The full well capacity is already passed by the fastest possible read-out at about 20% humidity.

The well-known chop-nod technique was applied throughout our observations. During the observations it became clear that the chopping f/35 secondary at the 2.2-m telescope is certainly not optimised for use at MIR wavelengths. The

---

[1] MANIAC is not an ESO instrument. It is described here because it is used on the ESO/MPG 2.2-m telescope at La Silla and it covers the same wavelength range as the ESO instruments VISIR and TIMMI2 described in the preceding article.

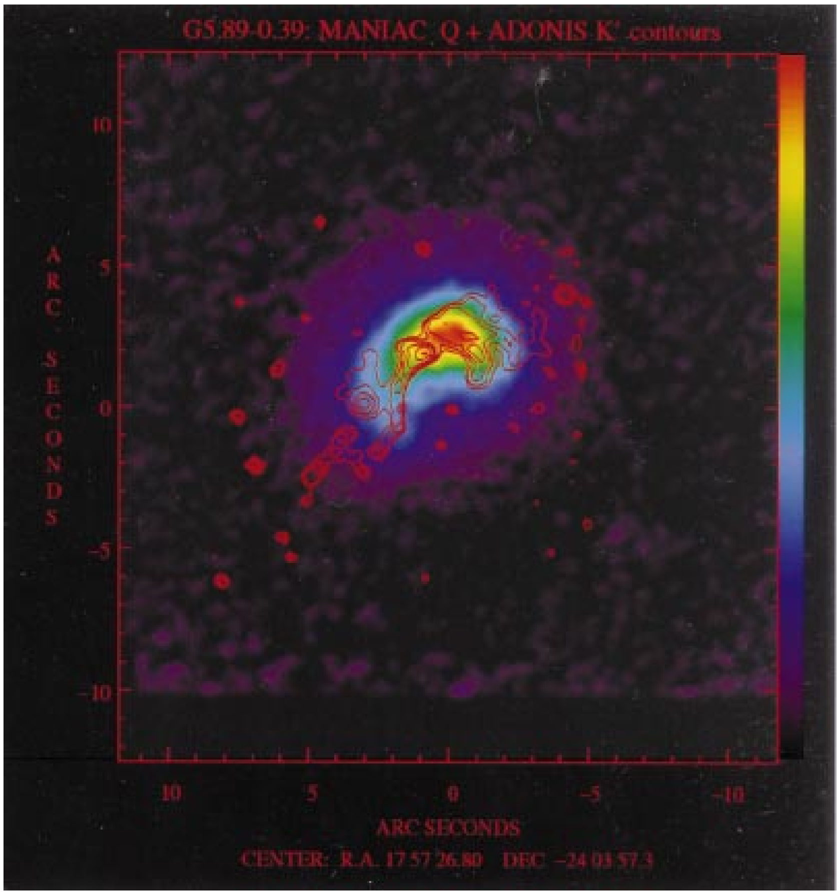

Figure 1: Mid-infrared Q-band image of the ultracompact HII region G5.89–0.39 with an overlay of near-infrared K′ contours.

chopper adjustment is quite critical with respect to the residual background structure in the final images. The best background cancellation level of about 10^{-5} was achieved by a combination of rotating and DC-tilting the secondary into certain positions, depending on the telescope zenith distance and hour angle.

First Results

Ultracompact HII Region G5.89–0.39

Using MANIAC at the 2.2-m telescope, the ultracompact HII region G5.89+0.39 was imaged for the first time in the Q band. Figure 1 shows our Q-band image tracing extended thermal emission from hot dust. We have overlayed contours representing near-infrared K′ data obtained with ADONIS/SHARP II (Stecklum et al., 1997). The K′ data delineate a similar overall banana-like structure quite different from the compact and more symmetric shell structure seen in the free-free radio continuum (Wood and Churchwell, 1989).

It is remarkable that the varying optical depth over one decade of wavelength from K′ to Q does not lead to a significant change of the morphology. This fact and the high surface brightness in the Q band indicate that the emission originates from an optically thick region. The lack of any infrared emission from the south-west part of the radio shell suggests an enormous extinction due to cold foreground dust. These features can be understood as signs of a very dense dust shell created by the interaction of both radiation pressure and wind from the central O6 star with the dense ambient remains of the parent molecular core. Obviously, the shell now starts to break-up.

Protoplanetary Nebulae

Stars in the post-AGB evolutionary stage are surrounded by a detached

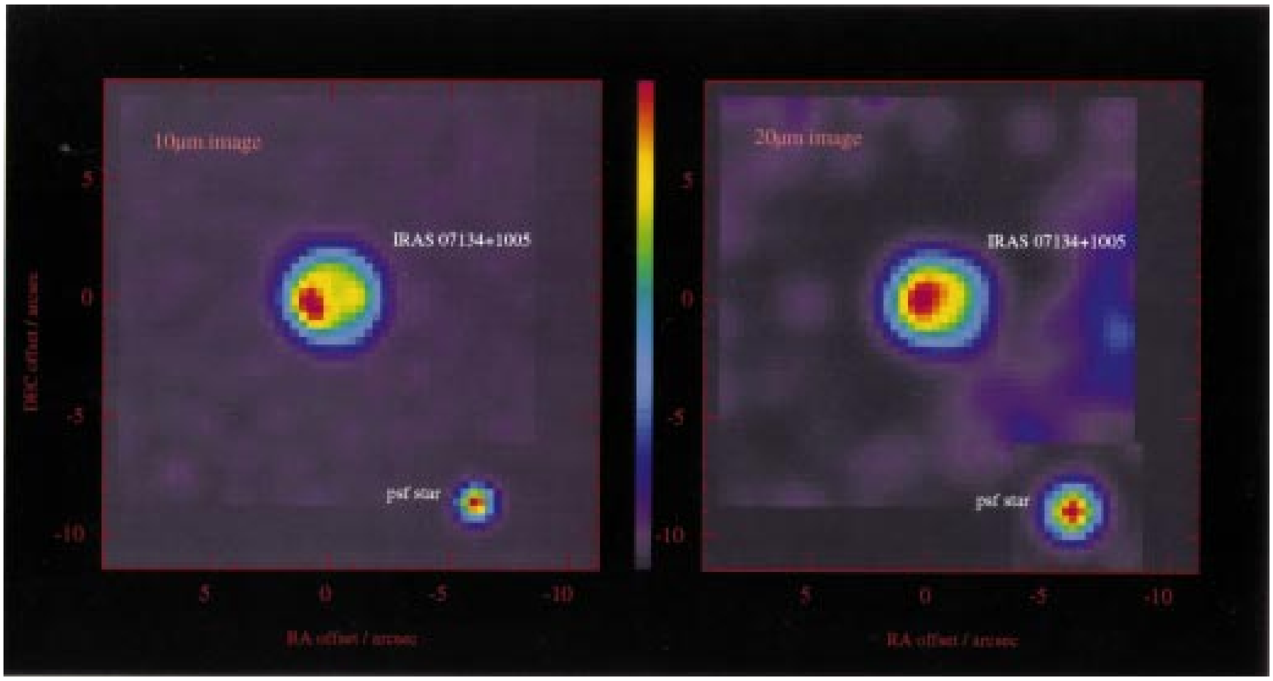

Figure 2: he protoplanetary nebula IRAS 07134+1005. The non-symmetric structure is seen both in the N-band image (left) and in the Q-band (right).

envelope of dust and gas. Due to their small angular extent, only little is known about the spatial structure of these envelopes. Using MIR cameras such as MANIAC, the emission of the warm dust particles located in the inner part of the dust shells can be spatially resolved. During the October 1996 observing run, a total of 5 objects have been searched for extended emission in the N and Q-bands; these data are in the process of being analyzed. As an example, we show in Figure 2 images of the post-AGB object IRAS 07134+1005. Extended emission is clearly seen in both images. Earlier results of this object have been published by Kömpe et al., 1997. We plan to compare the N and Q-band images with data at longer wavelengths and with the results of radiative transfer calculations modelling the spectral energy distributions of the objects.

Starburst Galaxy NGC 7552

One of the primary scientific goals for MANIAC are observations of galactic nuclei and their physical properties. As an example for the kind of data MANIAC can provide, we present in Figure 3 the N-band continuum image of NGC 7552, a southern barred spiral of Hubble type SBbc(s). Barred spirals very often show rings of molecular gas that are believed to form because of dynamical resonances between the orbiting molecular gas and the non-axisymmetric potential of the stellar bar. These so-called Lindblad Resonances often are the site of massive star formation and contain large amounts of warm dust. Our N-band image shows that the ring structure consists of various emission patches, presumably giant molecular clouds that are rotating around the dynamical centre. Such MIR data add important information to the detailed photometric and spectroscopic analysis of the central regions of galaxies. The goal is to develop reliable age determination methods for individual regions and to derive the evolutionary history of galactic nuclei. For the case of NGC 7552, this has been demonstrated in Schinnerer et al., 1997.

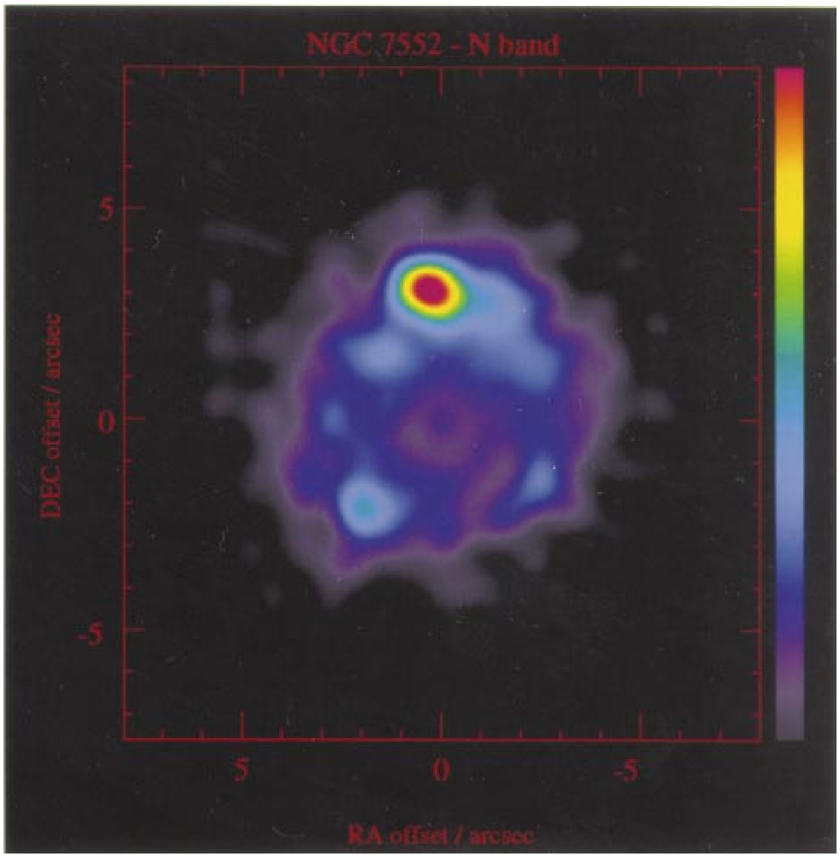

Figure 3: Star formation at the central region of the galaxy NGC 7552. Note that the integrated flux of the starburst ring in the N-band is only about 2.5 Jansky.

Acknowledgement

Commissioning a new instrument at any telescope is always a bit of a challenge. Both runs would certainly not have been so successful without the big efforts of the La Silla staff. We like to thank very much the 2.2-m Telescope Team for their support and for opening the telescope to daytime observation. Special thanks to the whole Infrared Group for all kinds of help, for their enthusiasm, and for many discussions.

One of us (TL) acknowledges the hospitality of the MPE infrared group while working in Garching.

References

Wood, D.O.S and Churchwell, E., 1989, *ApJS* **69**, 831.
Stecklum, B., Henning, T. Launhardt, R., Feldt, M., and Hayward, T.L., in prep.
Böker, T. 1996, PhD thesis, Max-Planck-Institut für Extraterrestrische Physik, Garching, Germany.
Böker, T., Storey, J.W.V., Krabbe, A., Lehmann, T., 1997, *PASP*, in press.
Schinnerer, E., Eckart, A., Quirrenbach, A., Böker, T., Tacconi-Garman, L.E., Krabbe, A., Sternberg, A., 1997, *Ap.J.,* submitted.
Kömpe C., Lehmann T., Gürtler J., Stecklum B., Krügel E.: Proc. IAU Symp. No. 180 on "Planetary Nebulae", Groningen, the Netherlands, August 1996 (in press).

Contact address: lehmi@astro.uni-jena.de

SOFI at the NTT

SOFI is currently being integrated in Garching with the goal of installing and commissioning it at the NTT by March 1998 and making it available to Visiting Astronomers in Period 61. This new instrument is a 1–2.5 μm imager/spectrometer which will offer:

- broad- and narrow-band imaging with a choice of pixel scales and maximum field of $5 \times 5'$
- polarimetry using a Wollaston prism
- long-slit grism spectroscopy at Rs 500
- cross-dispersed echelle spectroscopy at Rs 4000

Please check the ESO Web Site in July for further details on the capabilities of SOFI and information about its status and the Call for Proposals.

A. MOORWOOD, Garching, April 1997

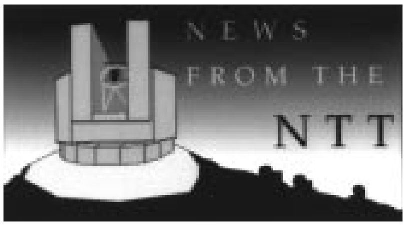

The NTT upgrade has the following goals:

1. *Establish a robust operating procedure for the telescope to minimise down time and maximise the scientific output.*
2. *Test the VLT control system in real operations prior to installation on UT1.*
3. *Test the VLT operations scheme and the data flow from proposal preparation to final product.*

J. SPYROMILIO, ESO

By the time you are reading this article, the NTT will have returned to full operations. At the time of writing we are in the final stages of the commissioning and tidying up of the control system. In May we will perform the last major software intervention on the telescope for the foreseeable future. This intervention is dominated by the installation of the May 97 release of the VLT control software and the Data Flow software release 1.0.

Since I last wrote for *The Messenger*, a few activities have been undertaken on the telescope side. We have made some improvements in the usability of the control system and introduced a number of software 'fuses' to improve the robustness especially in the areas of autoguiding and active optics. The telescope tracking is now within the specifications. Differential tracking has been verified with a number of exposures on comets. A large effort has been made on the instrumentation side. In particular the EMMI control software has been our efforts.

During the past few months we have also been working on the operational procedures for the telescope and the training of the operations crew in the use of the new control system. Although the operations crew has been involved in most aspects of the upgrade, it has been difficult for them to get extensive experience operating the telescope. In early February and the first half of March we ran the telescope in service mode. This gave us an opportunity to see the telescope and SUSI perform in a truly integrated manner and also to provide the operations crew with the necessary experience. A large number of problems were identified during this period, and some were rectified during the bright period at the end of March. In early April, during the dark period, further service observing with SUSI was undertaken. In late April, the telescope was taken off-line again to perform the first system wide tests of the EMMI control software. In early May and June we plan to perform some more service observations.

The overall performance of the telescope and instruments is good. We are still, at the time of writing, experiencing reliability problems with EMMI. These problems are being tracked down and resolved. On the SUSI side the system is robust. The commissioning of EMMI is proceeding at full speed and an extensive series of pre-planned tests are being undertaken. Although the instruments have not been changed, a number of small but very useful improvements to the software have now been tested. For example, the automatic focusing of the EMMI cameras based on the temperature of the instrument is now a tested and verified option. In any case, the days of using a calculator to work out the encoder value to drive the focus mechanism are over. The use of templates and phase 2 proposal preparation as an effective mechanism for using the telescope has been validated. The use of these tools to operate the NTT makes observing more efficient independently of whether you are working in classical or service mode. For this reason, we strongly encourage future users of the NTT to use the phase 2 proposal preparation software to build their observations before starting at the telescope. The software for P2PP runs in Garching and at the telescope and we aim to release it to the community at large during the next months.

In May, under the new release of the software, we will have an improvement in the usability of the Data Flow. New versions of the pipeline, archiving and P2PP software will be made available.

The May intervention is the last significant change to the NTT control system. The May 97 release of the VLT software contains a number of fixes to problems identified during the past six months and a number of general improvements in the robustness of the system. The NTT experiment has proved itself without a shadow of a doubt to be invaluable in the preparation of ESO for the VLT era. I wish to thank those of you who through your applications and your use of the P2PP software have helped us identify pitfalls and operational procedures that will make the system more effective. I believe that the NTT will prove to be useful for the community to prepare for the VLT era. During May we shall also be washing the NTT primary. According to the experience of the optics support team on La Silla this should make the NTT nearly as efficient as when the mirrors were realuminised almost ten months ago. In May we shall also be replacing the lamps in the Altitude and Rotator A encoders. The lamps have a finite lifetime and this is a standard maintenance operation.

During the upgrade we had hoped to install the CD-ROM writing hardware and software within the NTT. Unfortunately, we have been unable to deliver on this aspect of the NTT upgrade. For the time being, DAT tapes shall continue to be used until the CD-ROM software and hardware can be integrated into the La Silla wide operations environment. At the time I last wrote for *The Messenger*, we were aiming to start limited service observing with EMMI in April. As mentioned earlier, the EMMI commissioning did not start until mid-April. In addition, some of the Data Flow software to support the EMMI operations was not available at that time. We therefore had to limit the amount of observing we expect to be able to execute during the first half of period 59 to those programmes allocated the highest priority by the OPC. I apologise to those users that submitted applications but will not receive data. The instrument re-commissioning must take preference so that we can deliver the fully functional system to the astronomers in July. We had hoped to provide scientific access through the service mode at times during the re-commissioning. We achieved this for SUSI and aim to provide some scientific data for EMMI but, as mentioned above, shall not be able to execute all programmes that were submitted to the OPC for the first half of period 59.

Staff Movements

I would like to welcome Chris Lidman to the NTT Team. Chris who has been working already on La Silla with the IRAC cameras, has joined the NTT as the SOFI astronomer. I also take this opportunity to bid the NTT team farewell. I shall be leaving the team at the transition to full operations on June 27. The NTT shall then be in the capable hands of Gautier Mathys, who has had full responsibility for the day-to-day operations of the telescope for the past two years. My thanks and best wishes go out to all the team members, not only for doing a great job but making it fun also.

Jason Spyromilio
jspyromi@eso.org

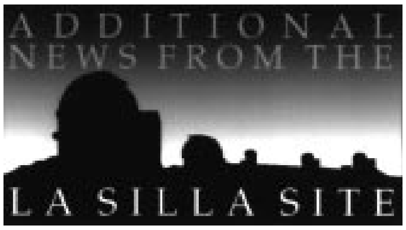

The La Silla News Page

The editors of the La Silla News Page would like to welcome readers of the seventh edition of a page devoted to reporting on technical updates and observational achievements at La Silla. We would like this page to inform the astronomical community of changes made to telescopes, instruments, operations, and of instrumental performances that cannot be reported conveniently elsewhere. Contributions and inquiries to this page from the community are most welcome. *(P. Bouchet, R. Gredel, C. Lidman)*

A New Fabry-Perot for IRAC2b

2.2-m AND IR TEAMS

During the next few months a new Fabry-Perot for IRAC2b will be tested and installed at the 2.2-m telescope. This Fabry-Perot replaces the current unit and promises improved performance. The new unit is flatter (λ/250 at 2 microns) than the current unit and covers a larger wavelength range (1.5 to 2.4 microns). Thus, in addition to what was possible with the old Fabry-Perot, observers will now be able to perform spectral line imaging with the new unit (together with the narrow-band filter, BP2) at 1.645 microns.

The new unit will become available during period 59. Observers who wish to use the new Fabry-Perot should check the IRAC2b home page http://www.ls.eso.org/lasilla/Telescopes/2p2T/E2p2M/IRAC2/irac2.html for test results as they become available. Alternatively, observers can contact the 2.2-m team at 2p2team@eso.org.

Load Cells Installed in the 3.6-m M1 Mirror Cell

R. GREDEL, S. GUISARD, G. IHLE

During two weeks of technical time in April, load cells were installed in the primary mirror cell of the 3.6-m telescope. This is the first major physical intervention in the mirror cell since the telescope became available. The aim is to improve the image quality of the 3.6-m telescope away from zenith, as described in the recent series of articles by Stephane Guisard in *The Messenger*.

On April 15, the mirror cell was removed from the telescope and then partly dismantled during the following days. All 30 astatic levers, the 3 axial fixed points and the lateral supports were removed from the cell.

The rubber of 18 pneumatic pads was replaced by material more commonly used for the production of pneumatic boats. The astatic levers and the lateral supports were modified in the workshop to house the load cells. That work was completed by April 28, when the mirror cell was re-installed at the telescope. Additionally, micrometers, which will allow the radial and axial displacement of the mirror within the cell to be measured, were installed. While work was done on the mirror cell, the mirror itself was taken to the aluminisation plant, where it was washed and freshly aluminised.

Image quality measurements were then performed during the following two nights. At the same time, all 30 astatic levers were checked. All but four levers were characterised by low hysteresis, of the order of 0.2 kg. Four levers showed huge hysteresis, up to 50 kg. At certain telescope positions, these levers were touching bolts of the cell structure or adjacent levers.

This problem may have existed for many years. The corresponding astatic levers were modified, and the hysteresis is now low for all of them. This ensures their proper functioning.

Direct images obtained with CCD#29 on April 29 resulted in some of the best images obtained so far with the 3.6-m telescope: 0.65–0.75 arcsec, with an outside seeing measured with DIMM2 of 0.5–0.7 arcsec.

The next major intervention is planned for September when the force distribution of the astatic levers upon the main mirror will be modified.

This requires us to measure simultaneously the aberrations away from zenith and the force on the load cells. These measurements will be carried out during forthcoming test nights allocated in June and August.

HIGHLIGHTS FROM THE KEY PROGRAMME
'A WIDE-ANGLE OBJECTIVE PRISM SURVEY FOR BRIGHT QUASARS'

The Hamburg / ESO Survey

D. REIMERS and L. WISOTZKI, Hamburger Sternwarte, Universität Hamburg

The Hamburg/ESO Survey is one of the important observational projects currently being carried out at La Silla whose objective is, among other things, to provide targets for the VLT (and HST).

1. Introduction

Bright quasars, in particular at high redshift, are an important tool of extragalactic astronomy and cosmology. Quasars can be used as light sources which probe intervening matter at cosmological distances and offer thereby a means to study the physical properties of distant gas clouds (abundances, ionising radiation) by high-resolution spectroscopy of absorption-line systems and of the Lyα forest. Notice that even with UVES at the VLT, a high-resolution spectrum of a 16th-magnitude QSO will require 10 hours integration time to reach a signal-to-noise ratio of 100. Such bright QSOs are also required for studies of absorption lines at $z > 2$ in the UV with the Hubble Space Telescope. Here we have to meet the additional

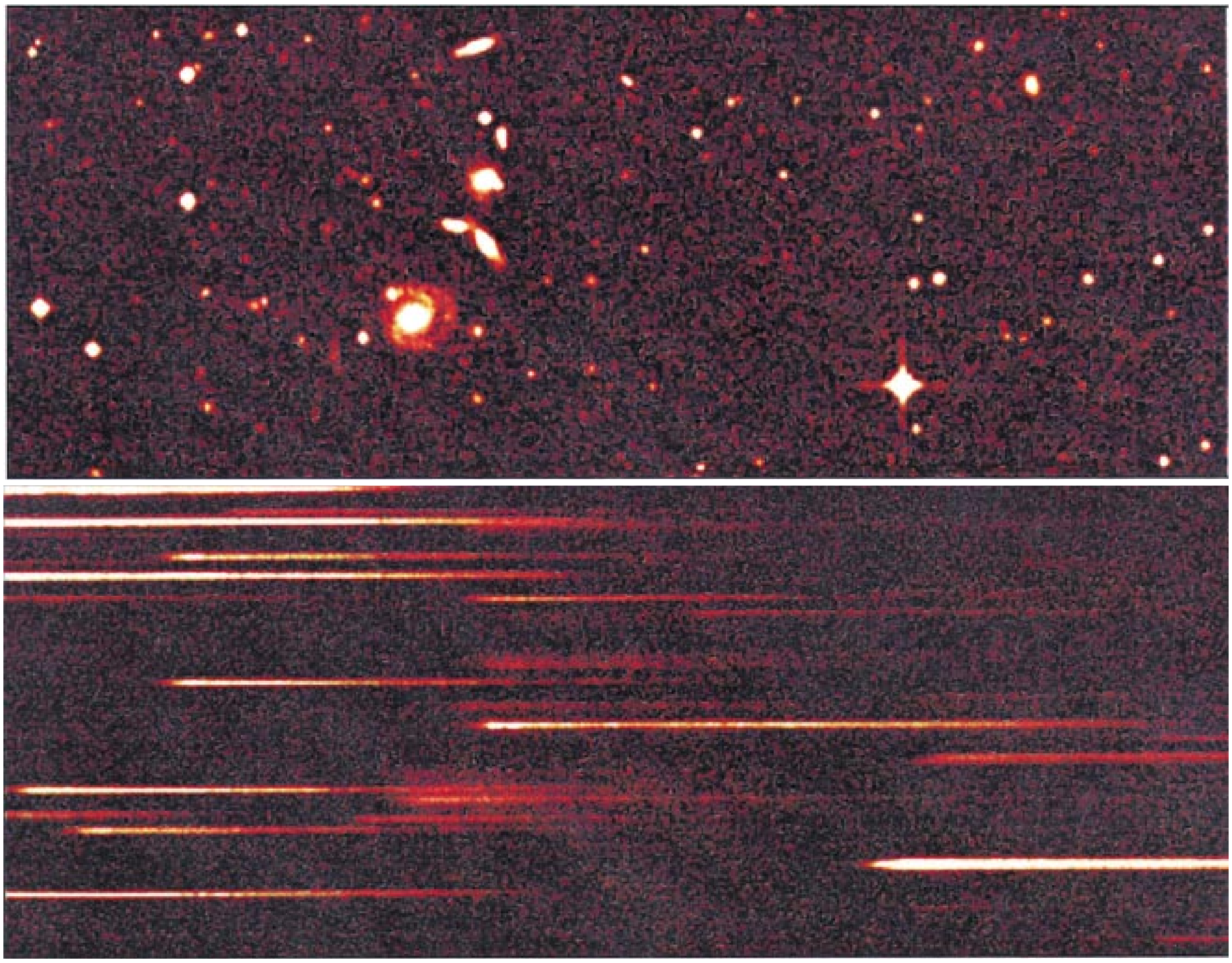

Fi ure 1: The area around the Seyfert 1 galaxy HE 0323–4204 (= ESO 301–G13; z = 0.058). In the upper panel, the direct image from The Digitized Sky Survey *shows* a *small group of interacting galaxies. The lower image is the corresponding section from the scanned objective-prism plate, with the sam image scale: In the centre, the Seyfert galaxy is conspicuous because of its long, blue spectrum (note that it is much sharper than the fuzzy spect a of the other galaxies, indicating its point source active nucleus); there are also some emission lines. The other objects are normal foreground stars.*

complication that for $z > 2$ due to absorption by optically thick Lyman limit systems of intergalactic matter, at most 20% of the lines of sight are transparent down to the shortest wavelengths observable with HST (1150 Å). This leaves us with the rather pessimistic (realistic) prediction that the whole sky may contain only 20 QSOs with $z > 2$ observable spectroscopically at resolution > 10^3 with HST in the UV (Jakobsen, 1995).

Among luminous QSOs there is also an enhanced probability to detect gravitational lenses. Surdej et al. (1993) found that among high-luminosity QSOs ($M_V < -29$) there is a chance of the order of 1% to discover a multiple image. Multiple QSOs offer the possibility to measure the Hubble constant H_0 via the time delay between images, to study the distribution of dark matter in the lenses and to measure the transverse sizes of absorbing gas clouds along the two light paths. The number of multiple QSOs truly gravitationally lensed is still small (≤ 20).

Since the rare bright QSOs can be found only by wide-angle surveys which cover basically the whole extragalactic sky, we proposed in 1989 to start such a survey for the largely unexplored southern sky using the ESO 1-m Schmidt Telescope equipped with an objective prism, in extension of an already running similar project in the northern hemisphere, the Hamburg Quasar Survey (Hagen et al., 1995), using the Schmidt telescope on Calar Alto (the former Hamburg Schmidt).

The prime scientific aims of the Hamburg/ESO survey as originally formulated (Reimers, 1990) are:

• to provide a sample of high-redshift QSOs for detailed absorption-line studies with the VLT;

• to search for further gravitational lenses (multiple QSOs);

• to find a few bright unabsorbed QSOs at EUV rest wavelengths suitable for He II 304 Å (the He II Lyα forest and the He II Gunn-Peterson test) and for metal abundance studies using EUV absorption lines;

• to provide a more complete QSO sample at the bright end since there was growing evidence that existing wide-angle QSO surveys like the Palomar-Green survey are rather incomplete.

As a by-product of the survey, we expected to find several interesting species of rare hot stars, e.g., exotic white dwarfs. While we gained experience conducting the survey, it became clear that several more objectives could be added to this list, among others:

• to directly determine the combined *local* (z 0) luminosity function of quasars and Seyferts;

• to investigate the evolution of luminous QSOs up to $z = 3$;

We hope to convince the reader in the following that we have indeed reached our aims.

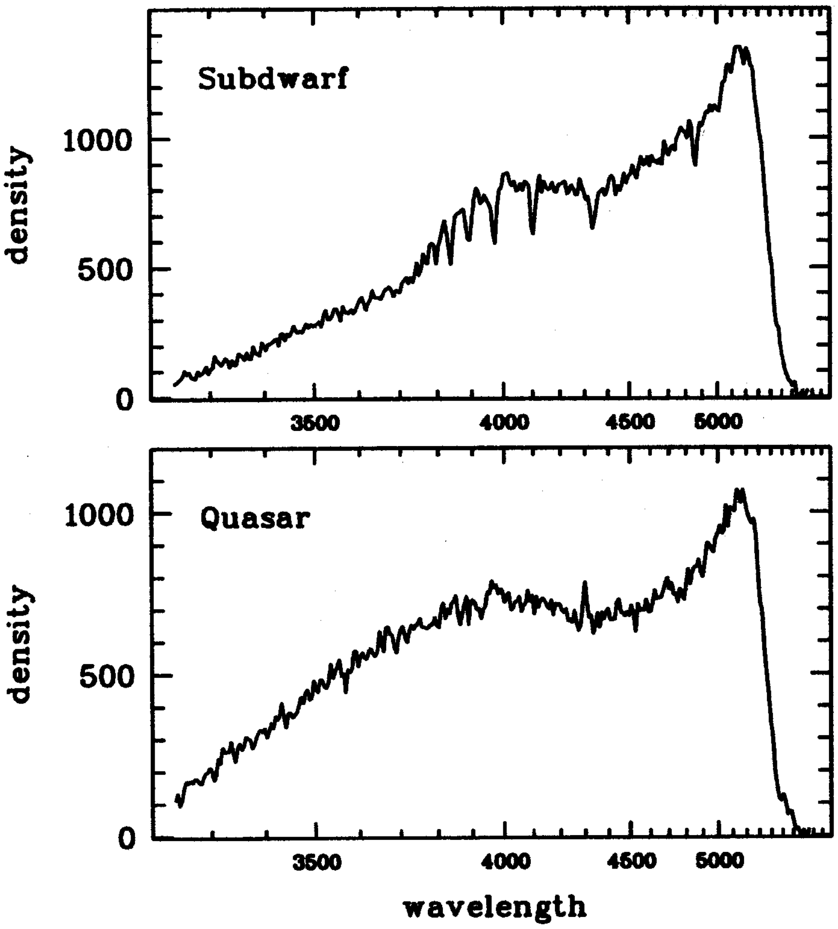

Figure 2: Example Schmidt spectra of two bright colour-selected quasar candidates, illustrating the power of using a high-dispersion objective prism. Note the non-linear wavelength scale. Ordinate is photographic density above diffuse background in arbitrary units. The sharp drop longward of 5400 Å is caused by the photographic emulsion. The narrow Balmer absorption lines clearly identify the upper object as a Galactic star. The lower panel shows a quasar at z = 0.15 (confirmed by slit spectroscopy): no stellar absorption is visible, and the only emission feature is a very weak and narrow [O II] line at a redshifted wavelength of   4300 Å.

2. Survey Procedure

The ESO Schmidt is one of the few large Schmidt telescopes with an objective prism. With 4° prism angle the dispersion is quite high (450 Å/mm at Hγ), and one might think this property makes it useless for extragalactic, especially quasar work where usually faint limiting magnitudes are to be achieved. However, it turned out that in a wide-angle survey for bright (B < 17. . .18) sources this was a lucky combination, as the spectral resolution in the prism spectra is high enough to unambiguously detect many stellar absorption features, and the quasar candidate samples scheduled for follow-up spectroscopy can be kept small (see Fig. 2). Recall that at B 16, more than 90% of just the UV excess sources are blue stars rather than quasars. With   5–6 magnitudes of dynamic range on the plates, we furthermore have essentially no *bright* limit: If there should exist a sister object to 3C 273 within the area covered by our plates, we are confident that we would find it (in fact, 3C 273 itself has already been 'rediscovered', see Fig. 4).

Performing an automated wide-angle survey using Schmidt plates requires the ability to digitise, store and process a large number of Schmidt plates on a reasonable time scale, with a minimum of human interaction. After an initial phase where we used an older digitisation and reduction scheme to select our candidates (described in Wisotzki et al., 1996a), we implemented in 1994 a newly-developed software package designed to preserve a maximum of information inherent in the plates while still keeping up with the requirement of high efficiency. In brief, the essential steps of the procedure are:

1. Object detection on digitised plates. Thanks to the availability of *The Digitized Sky Survey,* we have a 100% coverage of our objective-prism plates with a corresponding direct plate. This step yields a catalogue of typically   150,000 sources per Schmidt field. No morphological segregation is im-

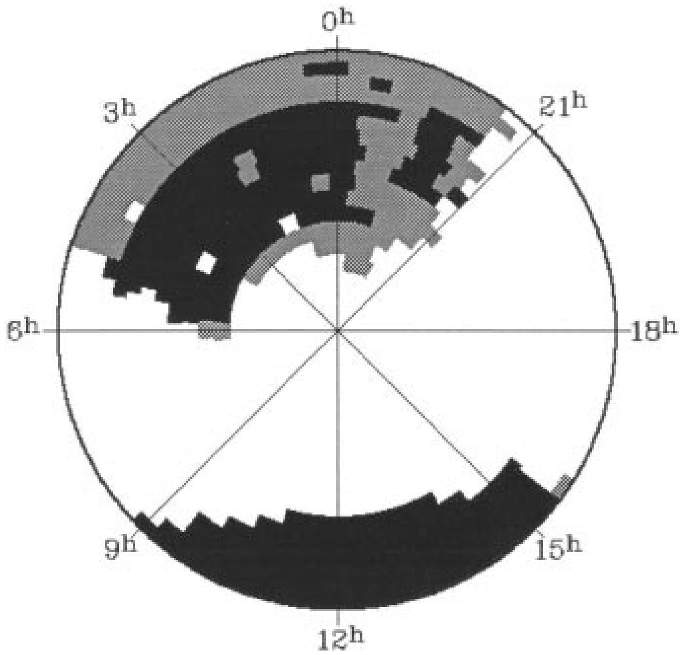

Figure 3: Distribution of available (shaded) and already digitised (black) ESO Schmidt objective-prism plates in the Hamburg/ESO survey, in azimuthal equal-area projection centred on the South Pole. The surrounding circle shows the equator ($\delta = 0°$), and octants are labelled by right ascension. The fields left white are in or too close to the Milky Way, except three plates still missing.

posed: both point and spatially resolved sources remain in the sample. This is important and quite different from most other QSO surveys; we do not wish to introduce biases against gravitationally lensed or low-redshift objects.

2. Full-plate scan of objective-prism plate in mapping mode with the PDS 1010G in Hamburg, requiring about 16 hours of scanning time. Each plate yields 430 MB of raw pixel data, archived permanently on CD-ROM. A small portion of such a scan, together with the corresponding section of the direct data, is shown in Figure 1.

3. Astrometric transformation from direct to spectral plate, providing an accurate (5 Å rms) wavelength zero point for each spectrum. Spectra locations contaminated by a nearby object are automatically recognised and flagged as 'overlaps'.

4. Optimal extraction of spectra from the digital data, giving 40,000 spectra above a minimum S/N ratio of 2 per plate, corresponding to a detection limit of B 18 ± 0.5 (depending on plate quality and seeing).

5. Candidate selection using a multitude of selection criteria:
- UV excess spectra;
- objects with 'blue' continuum slopes;
- emission-line objects;
- spectra with continuum breaks;
- dedicated Seyfert criterion.

Note that, contrary to a frequent belief, presence of emission lines is *not* essential for quasar candidate selection on digitised objective-prism plates; the large majority of quasars already satisfies the UV excess condition.

6. Remove 'false candidates', mostly stars and plate artefacts. This is the only partially interactive step in the procedure. At the same time, the remaining candidates are graded for follow-up observations. The 'completeness limit' is fixed one magnitude above the detection limit (i.e., at S/N 5). Below this limit, only *bona fide* QSO candidates, especially at high *z*, remain in the sample.

7. Snapshot slit spectroscopy of high-grade candidates using mainly the ESO 1.52-m telescope. An exposure time of 5 minutes is usually sufficient, yielding spectra with S/N > 15 for virtually all candidates. A success rate of 60–70% has now been achieved, with most of the non-quasars being peculiar blue stars.

3. Status of the Project

At the time of writing (April 1997), the mapping of the Southern extragalactic hemisphere by ESO Schmidt prism plates is essentially complete. Altogether, more than 460 spectral plates have been taken – just in time before the Schmidt telescope will stop to take IIIa-J glass plates. Plate digitisation, candidate search and follow-up spectroscopy are completed for more than 200 fields. Figure 3 shows the distribution of acquired and processed fields in the sky. About 650 new bright QSOs and Seyfert galaxies have been discovered, together with several hundred QSOs previously known in the fields. A first set of the newly discovered objects has already been published (Reimers et al., 1996a), and more will follow soon.

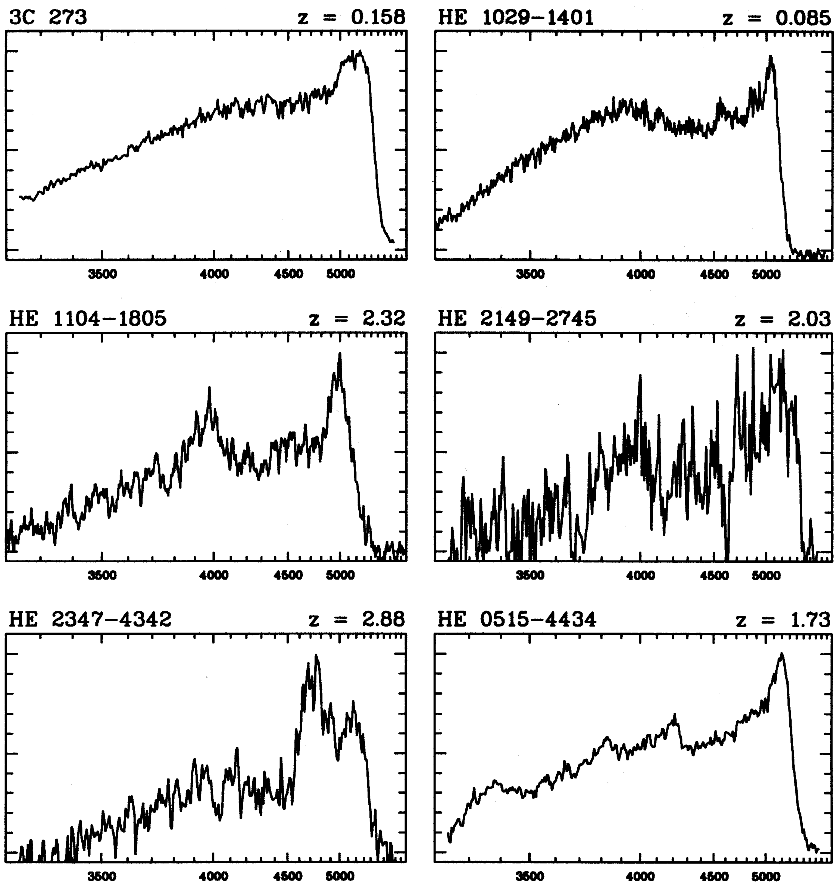

Figure 4: Portrait gallery with prism spectra of highlight objects featured in the text.

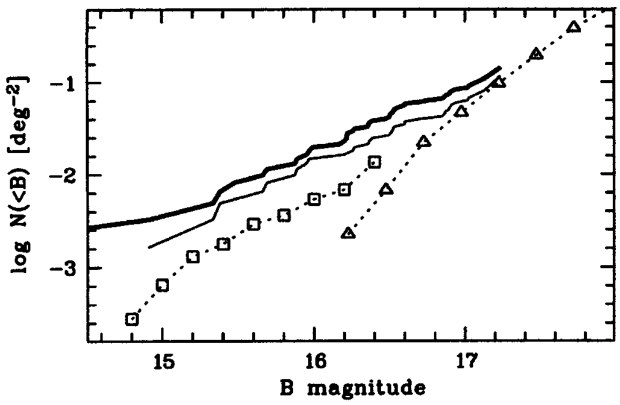

Figure 5: Cumulative surface densities of bright QSOs with z < 2.2. Thick line: Hamburg/ESO survey, z > 0.07, thin line: the same for z < 0.2. Open squares show the z > 0.07 counts from Schmidt & Green (1983), triangles give the LBQS (Hewett et al., 1995) relation, valid for z > 0.2.

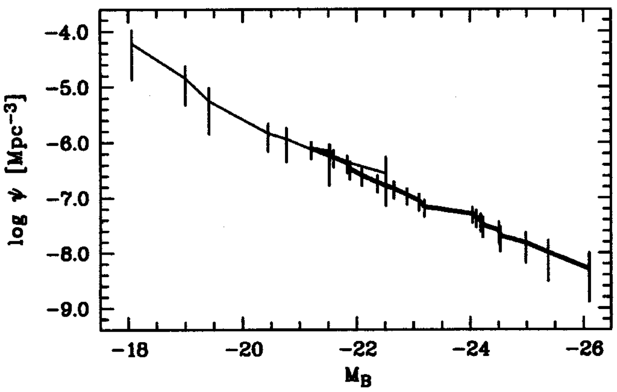

Figure 6: Combined local luminosity function of quasars and Seyfert 1 nuclei with z < 0.3, based on magnitudes corrected for the host galaxies.

In order to allow quantitative estimates of quasar surface densities and luminosity functions, we have launched a photometric calibration project for the Hamburg/ESO survey. Based on short B and V exposures made with the Dutch 90-cm telescope on La Silla, we are now able to give reliable magnitudes down to B 18–19 in already more than 300 fields; we expect to finish the calibration by the end of 1997 and shall then make the sequences available to the community.

In the following we highlight some of the most important results obtained during the last few years. In Figure 4 we present examples of objects, compiled from the database of digital objective-prism spectra. In this figure we additionally feature our two champions: 3C273 (= HE 1226+0219; B = 13.2, z = 0.158) and HE 1029–1401 (B = 14.1, z = 0.085), the two brightest QSOs in the entire sky.

4. Highlights

4.1 The local luminosity function of QSOs and Seyfert 1 nuclei

It is well known that quasars undergo strong evolution with cosmological epoch with a maximum in number density and/or luminosity at redshifts between z 2 and 3. Good knowledge of the local quasar luminosity function (QLF) is required for several reasons:

- Quasar evolution can be understood quantitatively only with a reliable zero-point at the present epoch.
- The interpretation of quasar absorption lines requires knowledge of the evolution of the metagalactic UV background radiation field which is itself due to quasars.
- Detailed studies of quasar properties, e.g., host galaxies or distribution of spectral properties, demand a complete local sample from which unbiased subsamples can be drawn.

In a first analysis, a complete flux-limited subsample has been constructed on a 600 deg^2 subarea of the Hamburg/ESO survey (Köhler et al., 1997). The two main results of this investigation are summarised in Figures 5 and 6. First, we find that the cumulative surface density $N(< B)$ of bright QSOs is much higher than in the Palomar-Green survey (PG; Schmidt & Green, 1983), by a factor 3 at B = 16, and by an even larger factor at B = 15, while it joins smoothly the relation from the LBQS (Hewett et al., 1995) for B > 17 (cf. Fig. 5). Our results confirm the suspicion raised by authors that the PG survey is highly incomplete.

Using this sample we have constructed the combined local (z < 0.3) luminosity function (LF) of QSOs and Seyfert 1 nuclei, the first such construction from a single survey in the literature. The cumulative LFs of luminous quasars and of low-luminosity Seyferts join smoothly (cf. Fig. 6), and both can be represented by the same single power law $\phi(L) \propto L^{\alpha}$ with α –2.2, without any indication of a break as demanded by the 'standard picture' of pure luminosity evolution. We find that the space densities of the most luminous QSOs (M_B < –24) are much higher in the local universe than hitherto assumed, as the Hamburg/ESO survey contains almost an order of magnitude more low-redshift QSOs per unit volume than the PG survey. The implication is that between z = 2 and z = 0 quasar evolution is much slower than assumed, and that the most luminous sources show the slowest evolution, in clear contradiction to the notion of pure luminosity evolution.

4.2 Gravitational lenses

HE 1104–1805: This new pair at z = 2.32 with 3.″1 separation (see also the

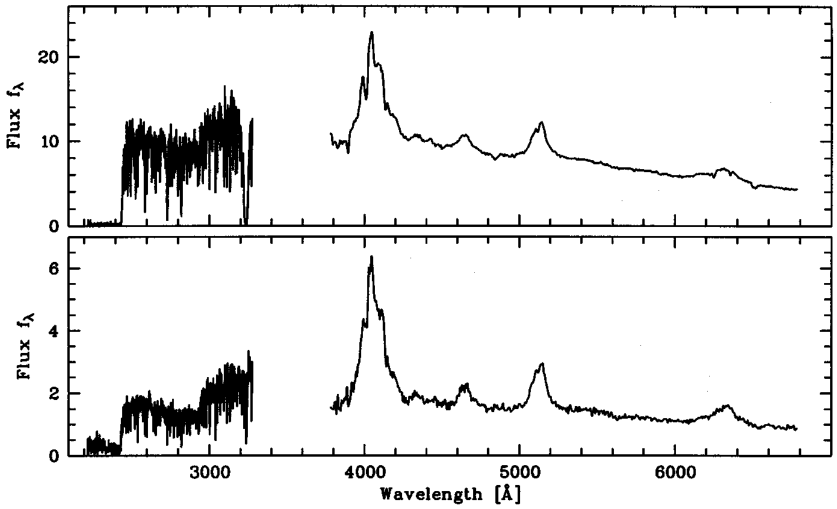

Figure 7: Optical and UV spectra of the two components of HE 1104–1805. The optical data were obtained with the ESO 3.6-m telescope and EFOSC1, the UV data with HST and FOS. Fluxes are given here, and in the following figures, in units of 10^{-16} erg s^{-1} cm^{-2} Å^{-1}.

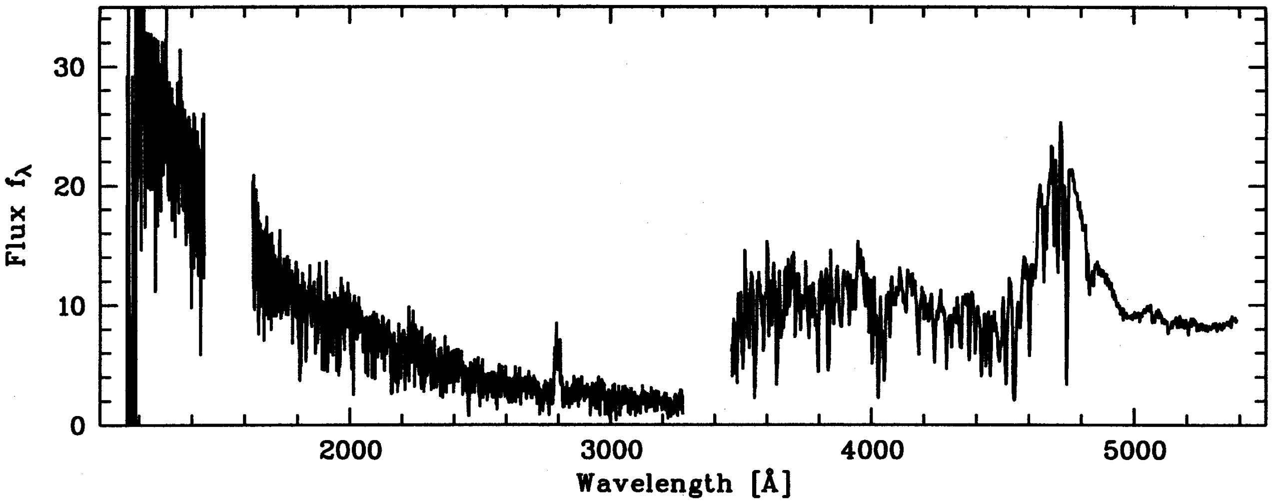

Fig re 8: Combined optical/UV spectrum of HE 2347–4342, obtained with the ESO/MPI 2.2-m telescope and EFOSC2, and with HST plus FOS (longer wavelengths) and GHRS (short wavelengths).

discovery report in *The Messenger* 72, 1993) is an exciting object for two different areas of research. Both components are bright enough for high-resolution spectroscopy (component A has B = 16.7, component B has B = 18.6) with the aim to determine the transverse sizes of absorbing clouds in the line of sight. Smette et al. (1995) have shown that the sizes of the Lyα clouds (about 100 such absorber systems have been detected) in the range $1.7 \leq z \leq 2.3$ must be larger than ≥ 200 kpc. Most interesting is a strong metal-line system at z = 1.66 which in A is a damped Lyα system with log N_H 20.8. Our HST spectroscopy with the FOS at $\lambda/\Delta\lambda$ = 1300 of both components shows that the same z = 1.66 system is a Lyman limit system in the line of sight of B with a non zero flux below the LL which allows to determine the hydrogen column density at log N_H 17.6 (Fig. 7). This is the first direct determination of the size of a damped Lyα system: the column density decreases by a factor of 10^3 over 20 kpc. This finding confirms the current picture of damped Lyα systems being 'galactic disks'.

HE 1104–1805 is also a remarkable gravitational lens system, not just a binary QSO. Our spectra taken in 1993 (Wisotzki et al., 1993) showed the two components with very similar spectral properties: identical emission line fluxes except a constant factor 2.8 between components A and B; however, the difference spectrum $f_A — 2.8 \times f_B$ reveals a hard and featureless excess continuum in A that could be due to selective amplification by microlensing by stars in the lensing galaxy. Spectra taken 1.5 years later confirm the gravitational-lens picture: Both components became fainter in the continuum with no changes in the emission-line fluxes (Wisotzki et al., 1995). It appears rather contrived to assume that two physically distinct sources show the same specific spectral variations, while the observed similarity of variations is a natural consequence of the gravitational-lens picture. The observed continuum excess in component A must be largely due to microlensing. Since 1995, we perform a regular spectrophotometric monitoring of this pair at ESO.

HE 2149–2745: This is a pair of redshift z = 2.03 BAL quasars separated by 1.″7 (Wisotzki et al., 1996b). The two spectra, with their highly specific broad P Cyg profiles and detached absorption troughs, appear identical except for a constant factor of 4.3, provide convincing evidence for the gravitational-lens hypothesis. The system is furthermore very interesting as the lensing galaxy has possibly been detected.

4.3 UV bright objects for spectroscopy with HST

Observing high-redshift quasars in the far UV is of key importance for the study of QSO absorption-line studies since the dominant ionisation stages of abundant ions (O III–O IV, NIII–N IV, Ne III–Ne VII, etc.), and the He I 584 and He II 304 resonance lines are in the intrinsic EUV part of the spectrum shifted to the HST range only in high redshift QSOs. However, a serious obstacle is posed by the cumulative free-bound absorption of hydrogen due to the numerous Lyα forest clouds and in particular the optically thick Lyman limit systems (see above).

All bright high-redshift unabsorbed QSOs known today (7 with z > 2) are from the Hamburg Quasar Surveys,

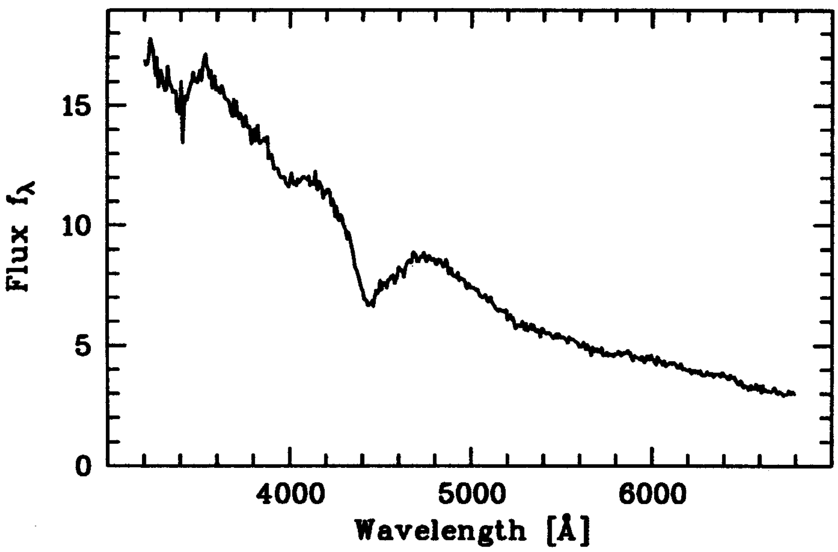

Figure 9: Low-resolution optical spectrum of the enigmatic object HE 1043–0502, taken with the ESO 1.52-m telescope.

and 5 of these have been observed in the meantime with HST. Besides HS 1700+6416 (z = 2.72) with its spectacular 'Lyman Valley' spectrum (Reimers et al., 1992) in which altogether about 40 new quasar absorption lines from the EUV have been discovered, allowing abundance studies in high-ionisation systems at high redshift, the most important object is **HE 2347–4342** (V = 16.1, z = 2.87). This bright QSO was discovered on La Silla in a follow-up run in October 1995 and observed with IUE to be unabsorbed down to at least 1200 Å in November 1995. With a flux of 3×10^{-15} erg cm^{-2} Å^{-1} s^{-1} near 1200 Å, HE 2347–4342 is a factor > 10 brighter than the two known z > 3 QSOs in which redshifted He II 304 Å absorption had been observed (Jakobsen, 1995). What had been seen so far was an absorption trough shortward of 304 Å in the QSO rest frame with the open question whether the detected He II opacity is solely due to unresolved He II forest line absorption, or contains a contribution from a diffuse IGM (the so-called Gunn-Peterson effect). Our June 1996 observations of HE 2347–4342 with the GHRS of the Hubble Space Telescope in its low-resolution mode ($\lambda/\Delta\lambda$ 2000) for the first time partly resolve the He II absorption (Fig. 8).

The rather spectacular He II absorption spectrum shortward of 1186 Å shows a succession of broad blacked-out "troughs" with no detectable remnant flux and "voids" with less than 50 per cent flux depression. Detailed modelling of the He II 304 Å forest using a high-resolution spectrum of the Lyα forest taken by Susanne Koehler in a 9-hour exposure with CASPEC at the 3.6-m telescope shows that while the "voids" can be explained by a combination of Lyα forest clouds with an additional small diffuse component ($\Omega_{\rm diff}$ < 0.02 $h_{50}^{-1.5}$ as a strict upper limit), the "troughs" can only be explained with the assumption of incomplete He II ionisation (Reimers et al., 1997). Apparently, He II reionisation is delayed compared to H ionisation and the expanding He III regions do not yet overlap at z = 2.9. In HE 2347–4342 we see for the first time the epoch of reionisation of the universe near z = 2.9.

A further highlight is the 1995 discovery of **HE 0515–4434**. With V = 15.1 and z = 1.73 it is the brightest known z > 1.5 QSO in the sky and among the most luminous objects in the universe. From IUE observations we know that between 2000 and 3000 Å it is also the UV brightest high-redshift QSO known and thus the best target for medium-resolution observations with STIS onboard HST of the Lyα forest in the largely unexplored redshift range 1 z 1.6.

4.4 Rare stellar objects

The combination of the relatively high spectral resolution of (depending on seeing) 10–20 Å FWHM of the ESO Schmidt objective-prism spectra with a limiting magnitude of 17 for visibility of stellar absorption features applied in a wide-angle survey offers the unique chance to detect stars with unusual spectra, in particular hitherto unknown types of stars. Since both AGN and stars with known absorption features (Balmer and Helium lines, Ca II H+K, ...) can be selected quite effectively, the not classifiable remaining objects have either no lines at all, or absorption spectra with very unusual wavelength patterns.

Among the latter we have found four magnetic white dwarfs with field strengths of several hundred Mgauss (Reimers et al., 1996b), and at least 3 further magnetic WDs with Zeeman triplets. Even more exotic is **HE 1043–0502**: Similar to GD 229 which probably has a He-rich atmosphere with fields above 1000 MG, it has broad, strong absorption features, none of which could be identified yet. We show the discovery slit spectrum in Figure 9, inviting the readers to guess about the physical nature of this object.

Another highlight has been the discovery of a new type of stars, with **HE 0504–2408** as one of their prototypes, namely DO white dwarfs with absorption lines of ultrahigh ionisation states like O VIII, Ne IX, etc. (Werner et al., 1995). According to their line profiles these lines must be found in expanding coronae of hot WDs.

5. Future Prospects

We expect to finish candidate selection and spectroscopic confirmation of candidates in about three years from now, where the time-limiting factor is mainly the digitisation of plates. More than 500 further new bright QSOs will be found, well timed to provide the community with a rich selection of objects for spectroscopy with UVES at UT2 of the VLT.

While the most interesting targets for VLT spectroscopy are presumably the high-z QSOs, the majority of quasars detected in the Hamburg/ESO survey will be at rather low redshifts, about 50% having z < 0.5. This will be an extraordinary pool to construct large and well-defined samples of highly luminous low-redshift QSOs, to study the relationship between QSOs, their environments, and their evolution in detail.

We have recently started developing a software package to classify stellar objective-prism spectra from their absorption lines, with the main intention to enable an efficient search for rare stellar types, irrespective of colour criteria. When applied to the final database of several million spectra, we will be able to construct complete samples of carbon stars, hot and cool white dwarfs of various subtypes, horizontal branch stars, etc.

Among the objects with no detectable stellar features we expect Halo stars with extremely low metal abundances ([Fe/H] < –3). Tests have shown already that we are indeed able to select such objects with good efficiency. It will be possible soon to provide larger candidate samples, in particular of the fainter unevolved objects, which can be observed with UVES with the purpose to study the chemical evolution of the first generation of stars in our galaxy.

Acknowledgement: We are indebted to H.E. Schuster, B. Reipurth, and G. and O. Pizarro for taking the Schmidt plates over seven years. Without the continuous support of the ESO staff this large project would have been impossible.

References

[1] Hagen H.-J., Groote D., Engels D., Reimers D., 1995, *A&AS* **111**, 195.
[2] Hewett P.C., Foltz C.B., Chaffee F.H., 1995, *AJ* **109**, 1498.
[3] Jakobsen P., 1995, in: QSO Absorption Lines, ed. G. Meylan, Springer-Verlag, p. 383.
[4] Köhler T., Groote D., Reimers D., Wisotzki L., 1997, *A&A*, in press.
[5] Reimers D., 1990, *The Messenger* **60**, 13.
[6] Reimers D., Vogel S., Hagen H.-J., et al., 1992, *Nature* **360**, 561.
[7] Reimers D., Köhler T., Wisotzki L. 1996a, *A&AS* **115**, 235.
[8] Reimers D., Jordan S., Koester D., Bade N., Köhler T., Wisotzki L. 1996b, *A&A* **311**, 572.
[9] Reimers D., Köhler S., Wisotzki L., Groote D., Rodríguez-Pascual P., Wamsteker W. 1997, *A&A*, in press.
[10] Schmidt M., Green R.F., 1983, *ApJ* **269**, 352.
[11] Smette A., Robertson J.G., Shaver P., Reimers D., Wisotzki L., Köhler T., 1995, *A&AS* **113**, 199.
[12] Surdej J., Claeskens J.F., Crampton D., et al., 1993, *AJ* **105**, 2064.
[13] Werner K., Dreizler S., Heber U., Rauch T., Wisotzki L., Hagen H.-J., 1995, *A&A* **293**, L75.
[14] Wisotzki L., Köhler T., Kayser R., Reimers D., 1993, *A&A* **278**, L15.
[15] Wisotzki L., Köhler T., Ikonomou M., Reimers D., 1995, *A&A* **297**, L59.
[16] Wisotzki L., Köhler T., Groote D., Reimers D., 1996a, *A&AS* **115**, 227.
[17] Wisotzki L., Köhler T., Lopez S., Reimers D., 1996b, *A&A* **315**, L405.

D. Reimers
dreimers@hs.uni-hamburg.de

Herbig-Haro Jets and their Role in Star Formation

BO REIPURTH, ESO, Observatoire de Grenoble

1. Half a Century of Herbig-Haro Research

In the late forties, George Herbig of Lick Observatory and Guillermo Haro from Tonantzintla Observatory, Mexico, independently discovered some curious semi-stellar objects in Orion with unusual emission-line spectra. Although it was early on realised that these mysterious objects were somehow related to star birth, for several decades progress in understanding their nature was slow. A major breakthrough occurred in the mid-seventies when it was realised that the characteristic HH spectra, because of their similarity to certain supernovae spectra, could be understood in terms of shocks. Shortly afterwards, it was discovered that HH objects have major proper motions, with vectors pointing away from very young stars. Finally, in the early eighties, it was realised that some HH objects could take the form of highly collimated jets. With those results the scene was set for an explosion in HH research which has continued unabated till today. Indeed, HH flows are now recognised not only as fascinating astrophysical laboratories involving shock physics and chemistry, hydrodynamics and radiation processes, but it has gradually been realised that HH flows hold essential clues to the birth and early evolution of low-mass stars. A few months ago, an IAU Symposium[1] was held in Chamonix in the French Alps, where a total of 178 researchers from 26 countries met to discuss our present level of understanding of Herbig-Haro flows and their relation to disk accretion events and T Tauri winds and other outflow phenomena like molecular outflows, embedded molecular hydrogen flows and radio jets.

During the 11 years that I have worked for ESO in Chile, I have had the opportunity to use world-class instrumentation in the superb observing conditions of La Silla. As I leave ESO to return to academia, I would like to summarise some of my scientific activities of the recent years. In the following pages I will review the status of HH research, with an unapologetic emphasis on my own interests and results.

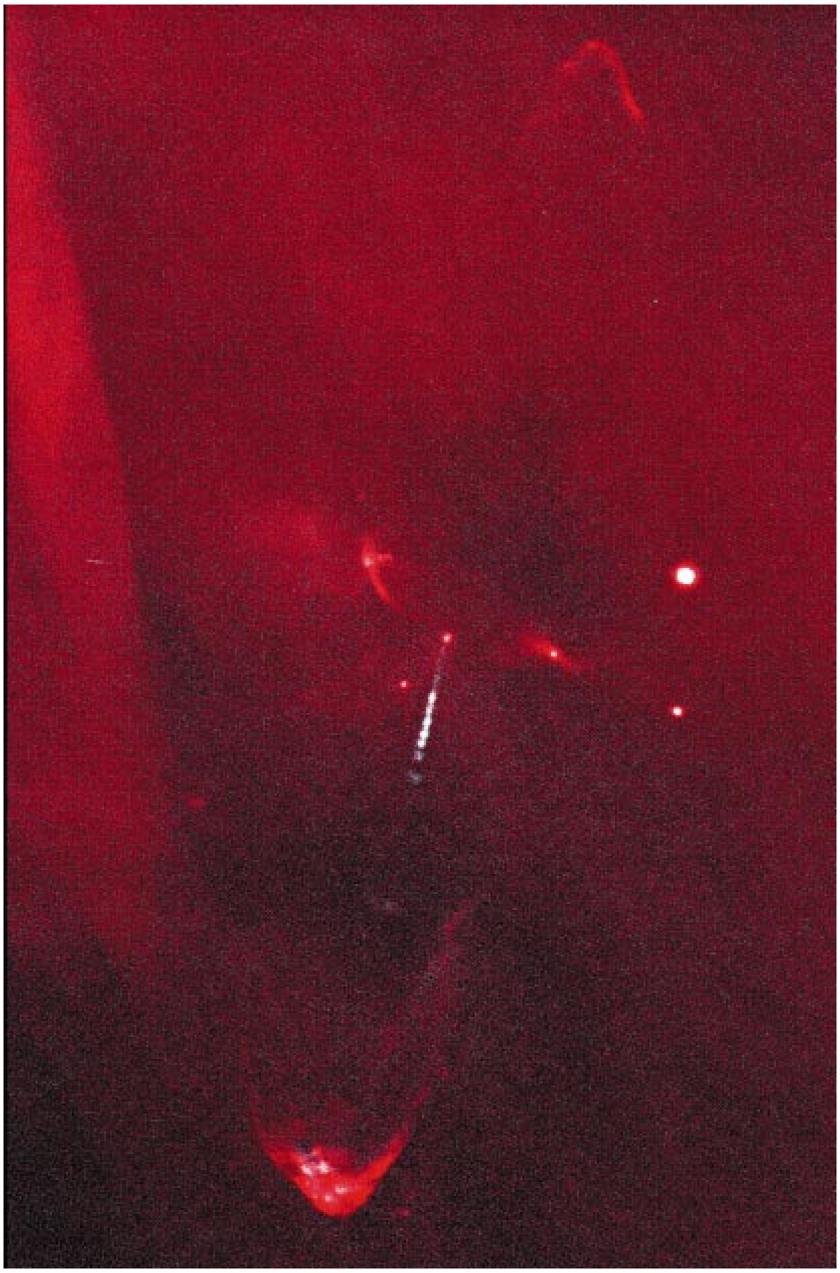

Figure 1: NTT image of the HH 34 jet. Red is Hα strong, and white is [SII] bright.

2. The HH 34 Jet

Figure 1 shows an Hα and [SII] composite CCD image obtained at the NTT, showing the HH 34 jet complex. This jet displays the basic features of HH flows, although rarely are they seen as clean and neatly as in this case. Located in the molecular clouds in Orion at a distance of 460 pc, the jet consists of a chain of compact emission knots which emanate from a faint young star. The jet points straight towards a large bow shock, which marks the point where the supersonic flow rams into the ambient medium. The effect of this 'working surface' is to decelerate the fast jet material and to accelerate the ambient medium.

[1]Herbig-Haro Flows and the Birth of Low Mass Stars, IAU Symposium No. 182, eds. Bo Reipurth and Claude Bertout, Kluwer, in press.

On the opposite side of the driving source and symmetric with the southern bow shock, one finds a fainter counter bow shock. Together the two lobes form a bipolar outflow with an overall extent of 0.4 pc. The southern lobe is approaching us, while the northern recedes. The absence of a collimated counterjet could therefore be ascribed to heavy extinction in the cloud core surrounding the young source, but infrared observations have failed to find evidence for an embedded jet, so it seems likely that the absence of a counterjet is real, a fact that is not easily understood.

Images taken at the NTT on different epochs with several years in between clearly show proper motion in the jet and its bow shock [1]. This way one finds that the flow propagates with a velocity of more than 200 km/sec. When combined with radial velocities determined from long-slit spectra, we find that the flow has an angle of 28 degrees to the plane of the sky.

The particular region of the Orion dark clouds where HH 34 is located is rich in other Herbig-Haro objects, which have been known for some time. A few years ago, it was realised, much to the surprise of the star-formation community, that many of these other HH objects in fact form part of a single giant HH complex, stretching over almost 3 parsecs, and driven by the little faint energy source at the base of the jet [2]. As will be discussed in section 5, the existence of such parsec-scale jets has opened up a discussion about the role of HH jets in creating turbulence and chemically processing the interstellar medium.

3. The HH 47 Jet

The large Gum Nebula in the southern sky is excited by several massive and very luminous stars. The effect of these stars on the pre-existing molecular clouds has been rather devastating, and all over the Gum Nebula one finds windswept cometary globules, which are the remains of larger tenuous cloud complexes that have now been swept away, exposing the surviving denser cloud cores. Sometimes during these violent processes, star formation can be triggered. One such windswept Bok globule with a new-born star inside is seen in an Hα+[SII] image from the NTT in Figure 2. A spectacular bipolar jet, HH 47, is seen to emanate from an embedded young star. Thanks to the efficient removal by the strong UV radiation of the cloud material normally shrouding a cloud core, we here have a view of unprecedented clarity of a bipolar HH jet. The geometry and kinematics of the flow are very similar to the HH 34 flow, and suggest a dynamical age of the system of about a 1000 years [3]. The bright jet is located in the approaching lobe, escaping from the globule, while the red lobe burrows into the interior of the globule, and only a faint heavily obscured counterjet is visible.

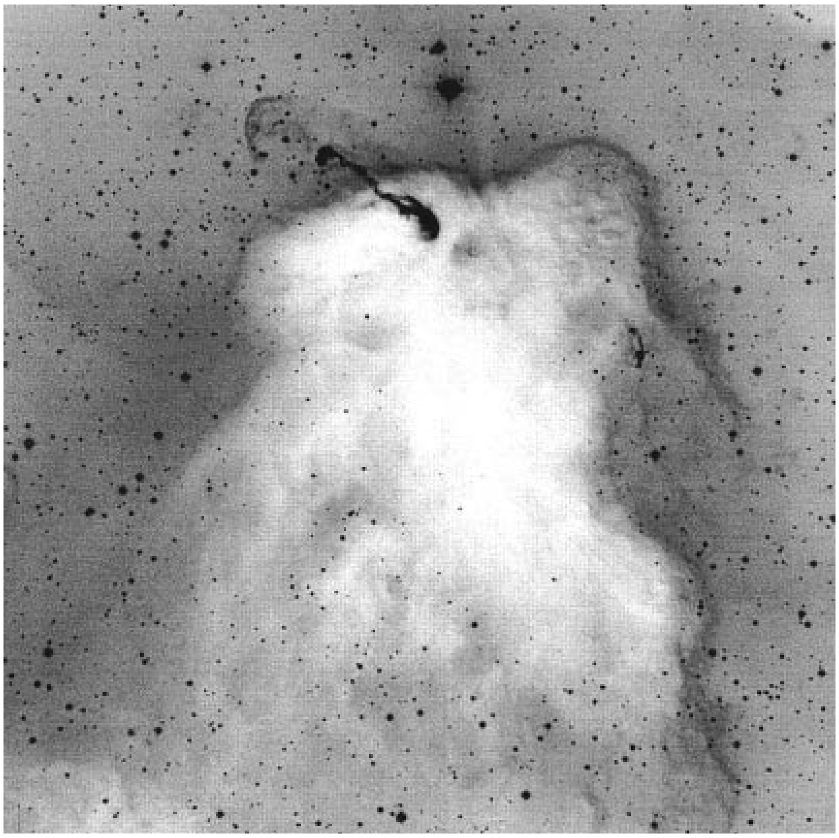

Figure 2: Hα + [SII] NTT image of the HH 47 flow.

The NTT images represent the best that one can do from the ground, so the natural next step was to observe it with the Hubble Space Telescope. We have obtained deep exposures of the HH 47 jet with the HST in Hα and [SII], providing a resolution almost 10 times better than that of the NTT images [4]. Figure 3 shows a colour composite of the main body of the HH 47 jet, with Hα bright regions seen in blue and [SII] bright areas in red. The white curved nebula at the bottom of the jet is a cavity which the jet has dug out of the globule and which is illuminated by the nascent star. Close examination of the image reveals that the jet has two spatially separated components. One is a series of [SII] bright knots, which form the body of the jet, as it winds its way outwards from the globule. Another is an Hα bright fine web of narrow filaments, which are predominantly located at the edges of the jet. It is apparent that the most prominent of these Hα filaments trail behind knots in the body of the jet like the wings of miniature bow shocks, and they often occur at points where the jet shows kinks or shoulders.

It is highly improbable that the jet actually follows the complex path seen in these images. Rather, once the central engine has spewed out a blob of material, it will continue ballistically. Therefore, the winding structure of the jet must reflect a wandering, or irregular precession, of the direction of the ejection axis of the young star. The difference in morphology of the HH 34 jet in Figure 1 and the HH 47 jet in Figure 3 is likely due to a difference in the amplitude of the directional variations of the flow axis: in HH 34 the flow axis is very stable producing a narrow straight jet, whereas in HH 47 the ejection axis roams around producing a wiggling jet.

Fabry-Perot observations of the HH 47 jet reveals that the outer cocoon of the jet body flows slower than the inner parts, much as a viscous fluid passes through a tube [5]. This suggests that the jet may be entraining material and is transferring momentum to the ambient medium as it progresses outwards. The HST images reveal that this process occurs through the collective effect of a succession of small internal working surfaces. As they sweep up and accelerate the ambient gas, the surroundings of the jet is set into motion, which we can observe as one of the molecular outflows so commonly found in star-forming molecular clouds.

At the end of the jet we see a major bright bow shock. Here both ambient material and jet material are shocked, mixed and ejected sideways, and similarly to the smaller shocks around the jet body, this helps to set the ambient medium into motion. Examination of the

Figure 3: The HH 47 jet as seen with HST. Red is [SII] strong, and blue/green is Hα bright.

ratios and profiles of the emission lines emitted from the bow shock tells us about the shock velocity of the material there. When compared to the physical velocity of the bow shock derived from proper motions and radial velocities, one finds that the material velocity is much higher than the shock velocity. This can only be understood if the jet is moving into a medium that has already been set in motion by the previous passage of one or more earlier bow shocks. As can be seen in the wider field image in Figure 2, a large faint bow shock is indeed visible further out on the flow axis.

4. The HH 111 Jet

The HH 111 jet, together with the very similar HH 34 jet, is the object which comes closest to the text book idealisation of how a jet should look. Consequently, it has been the subject of intensive study using the full gamut of observational techniques and has become one of the favourite bench marks against which theoreticians test their models.

Figure 4 shows a composite of deep Hα and [SII] images taken with the ESO 3.6-m telescope. The jet emerges from a young star deeply embedded within a compact molecular core in the L 1617 cloud complex in Orion [6]. The jet has a bright body, terminating in a bow shock, followed by a series of fainter bow shocks, until it fades from view, only to appear again in a bright bow shock, called V, located 0.3 pc from the source. The jet and V are both blue shifted. Proper-motion and radial-velocity measurements show that they recede from the source with a space velocity of about 400 km/sec and that the flow is inclined at an angle of only 10 degrees to the plane of the sky [7]. On the opposite side of the source from V, a counter jet and a pair of bow shocks, HH 111 X and Y. trace the red-shifted lobe of the outflow. At optical wavelengths the counter jet is

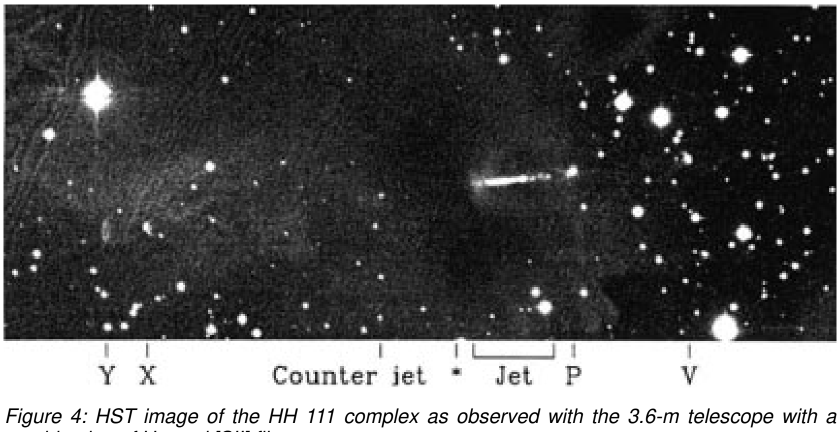

Figure 4: HST image of the HH 111 complex as observed with the 3.6-m telescope with a combination of Hα and [SII] filters.

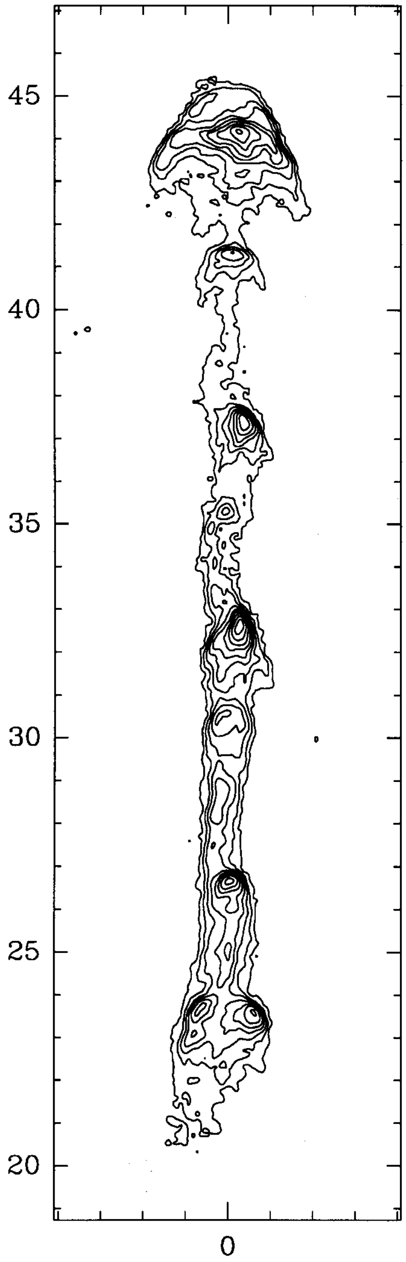

Figure 5: Contour diagram of the body of the HH 111 jet from an Hα HST image.

Figure 6: A mul itude of HH flows can be seen in this wide-field image of the young cluster NGC 1333 taken at the 0.9-m telescope at Kitt Peak.

highly obscured and consequently faint. However, in the infrared the jet shows a remarkable symmetry [8]. The entire complex spans a length of 0.8 pc.

The driving source, IRAS 05491+0247, is deeply embedded in the cloud core, with a luminosity of 25 L and is surrounded by large amounts of cold dust and gas. It is detected in the centimetre radio continuum, and high-resolution VLA maps reveal a small, only 1″ long, radio jet precisely along the axis of the much larger optical jet. Since we know the velocity of the jet, we can deduce that the radio jet is only about one year old, in other words, the star is actively producing the jet at this very moment. The source is presumably a binary, since another jet, only seen at infrared wavelengths, emanates from the source at large angles to the HH 111 axis [8].

The HH 111 complex is associated with a major molecular outflow, consisting of a very large red lobe, where the flow skirts through the southern edge of the L1617 cloud, and a much shorter blue lobe, where the flow escapes from the cloud. Higher-resolution ^{12}CO observations show that the blue lobe is a well-collimated CO jet co-axial with the HH jet [9].

In a detailed spectroscopic analysis of the principal bow shock V, it was found that the ambient medium ahead of the bow shock flows away from the source with a velocity of 300 km/sec [7], which suggests that the bow shock V is not the outermost bow shock, but must have been preceded by even earlier ejecta. This was confirmed when three high-velocity CO bullets were found further out along the jet axis. None of these three bullets are visible optically, but because of their very high space velocities, similar to that of the optical jet, it follows that they are also part of the jet complex.

Figure 5 shows a contour diagram of our Hubble Space Telescope image of the body of the HH 111 jet taken through an Hα filter [10]. The image provides a wealth of new information on the jet structure. The jet appears to be fully resolved perpendicular to the flow direction, and the knotty substructure is rich and complex. The body of the jet terminates in a bright knot, L, which has an

Figure 7: An Hα image of the HH 110/270 flows obtained at the NTT.

obvious bow-shock morphology. In the body of the jet, most of the brighter knots also have bow-shock shapes, with a compression in the contours in the flow direction. Bow shock wings sweep backwards on either one or both sides of the bright knots. At the base of the jet, where it emerges from the dense cloud core surrounding the embedded star, another large bow shock, E, is just about to appear. Apart from these two bright bow shocks, the jet maintains a fairly constant width along its axis, averaging about 0.8″, or 350 AU. The image provides strong support for the notion that knots in HH jets consist of small bow shocks. Since the HH 111 jet is almost perfectly straight, with only a minor wiggling, directional variability is not nearly as important an influence as for the HH 47 jet, and the knots are therefore likely to form as fast jet material overruns slower jet material.

In a recent study, we have searched along the well-defined jet axis for more distant bow shocks, and quite to our surprise we found two large working surfaces each located half a degree on the sky from the source [11]. We have convinced ourselves that they are indeed part of the HH 111 complex, because not only are they lying precisely on the jet axis and are perfectly symmetric around the source, but our proper-motion measurements show that they each move away from the source with highly supersonic velocities. With an angular extent of almost 1 degree, corresponding to 7.7 pc at the distance of Orion, HH 111 is the largest known HH flow in the sky!

5. The Impact of Jets on their Ambient Medium

Following the discovery of giant HH flows at HH 34 and HH 111, we have made a systematic search for other giant HH flows, using the ESO Schmidt telescope in the southern sky, and the Kitt Peak 0.9-m telescope equipped with a large-field CCD for the northern hemisphere. We now have recognised of the order of 20 parsec-scale HH flows, suggesting that such enormous extents are common properties of HH jets. This has important implications for our understanding of the underlying physics of mass-loss phenomena from new-born stars, and their effect on the surrounding interstellar medium. Firstly, since shocks in parsec-scale flows trace ejecta that are progressively older with increasing distance from the source, it may be possible with detailed studies of such gigantic flows, at least in part, to reconstruct the mass-loss history of the driving source. Secondly, when fast shocks propagate through the interstellar medium near or between molecular clouds, they may dissociate molecules and return the medium to its atomic state, which may help to explain the large observed abundances of species like C I and C II found even where there is no UV radiation from massive stars. Thirdly, HH flows may be an important source of momentum and energy injection into their parent clouds, and they may be able to contribute to the turbulence measured in dark clouds. This again may lead to self-regulation of star formation.

A stunning case of how star formation can transform a dark cloud is seen in Figure 6, which shows an Hα+[SII] wide-angle (23 arcmin) CCD image of the NGC 1333 molecular cloud in Perseus [12]. Hα emission is red and [SII] is blue-green. A cluster of about 150 low- to intermediate-mass young stars have been found by infrared surveys in the cloud. Many of these new-born stars are actively forming outflows, and our image shows over 30 groups of HH objects driven by over a dozen young stars. The density of HH flows in this cloud is so high that flow confusion becomes an important issue. Some HH objects are seen well outside the boundary of the opaque cloud, and may be part of giant HH flows, which have burst out of the cloud, and now dump their kinetic energy into the surrounding interstellar medium. The flows show a great variety of morphologies, from amorphous structures to the exceedingly collimated HH 333 jet towards the top of the image, which has a length-to-width ratio of over one hundred!

When flows are ejected from their energy sources, they are not always allowed to coast in a straight trajectory. Molecular clouds are highly complex structures, and if a sufficiently dense cloud core is blocking the way for a jet, rather spectacular fireworks may result. Figure 7 shows an Hα+[SII] mosaic of the HH 110 flow in Orion, obtained at the NTT [13]. This flow was for years puzzling, because despite its rather well-defined structure it was impossible to find an energy source along the flow axis. But when a deep image was taken at the NTT, it became evident that there is a second much fainter flow in the region, called HH 270, to the north-east of HH 110 and with an axis pointing towards the apex of HH 110. A proper-motion study revealed that the HH 270 flow is moving with a speed of 300 km/sec directly towards the beginning of the HH 110 jet. The only possible explanation is that the HH 110 flow is the result of the HH 270 flow suffering a grazing collision with an obstruction. The result of the collision is that the high-velocity gas in the HH 270 flow (only part of which is shocked and therefore rather faint) suffers a strong shock while being deflected, and re-emerges as the bright and complex HH 110 flow. The molecular cloud from which HH 110 is seen to emanate is a natural candidate for this obstruction, and indeed, mm observations at the SEST have revealed a cloud core just north-west of the beginning of the HH 110 flow.

6. Jets and the Birth of Stars

Studies of HH energy sources have shown that, as a class, they are among the youngest stars known, and that they are still surrounded by massive envelopes of cold gas and dust [ref.]. Besides that, little is known about these sources and what triggers their spectacular outflows. One important clue comes from the multiple working surfaces found in many HH flows, which suggests that the sources suffer multiple eruptions.

One class of eruptive variables known among young stars is the group of FUors, so named after the prototype FU Orionis. These stars are believed to be ordinary late-type T Tauri stars which undergo brightenings of 5–6 magnitudes and emerge with F–G supergiant optical spectra, while in the infrared they have late M-type spectra with very deep CO absorption bands. This behaviour has been successfully modelled as events of increased accretion through circumstellar disks at rates significantly larger than for ordinary T Tauri stars [14]. The entire disk heats up and becomes self-luminous, and the light from the disk completely swamps the light from the central T Tauri star. Because disks are low-gravity environments they show supergiant features in their spectra, and because they have a temperature gradient outwards from the star, solar-type spectra will dominate in the visual, whereas infrared observations will probe much cooler parts of the disk and show much later spectral characteristics. In their high states, FUors are luminous objects and their spectra show pronounced P Cygni profiles revealing that they possess massive, very high velocity winds.

It has been suggested that FUor events are responsible for the multiple shocks seen in HH flows [15, 6]. Is there any observational evidence to support this contention? Not many FUors are known, and the latest compilation lists only 9 objects. Of these, 3 are associated with HH objects. No other class of young stars have anywhere near such a high percentage of association with HH objects, and yet most HH energy sources are, when they are at all observable in the optical, T Tauri stars. This seems to contradict the idea that FUors should drive HH flows. However, it can be understood when one considers the time scales involved. FUor events are repetitive, and although their frequency of outburst is poorly determined, it appears that they decay to their low, presumably T Tauri, state on timescales of the order of a century or more, but with a large spread for individual objects. The dynamic timescales of the bow shocks in well-defined jets like the HH 34, 47 and 111 jets we have just been discussing, are of the order of 500 years or so. Therefore, whenever we observe an HH energy source, it is more likely to have already decayed into its T Tauri state than to still be in a FUor state.

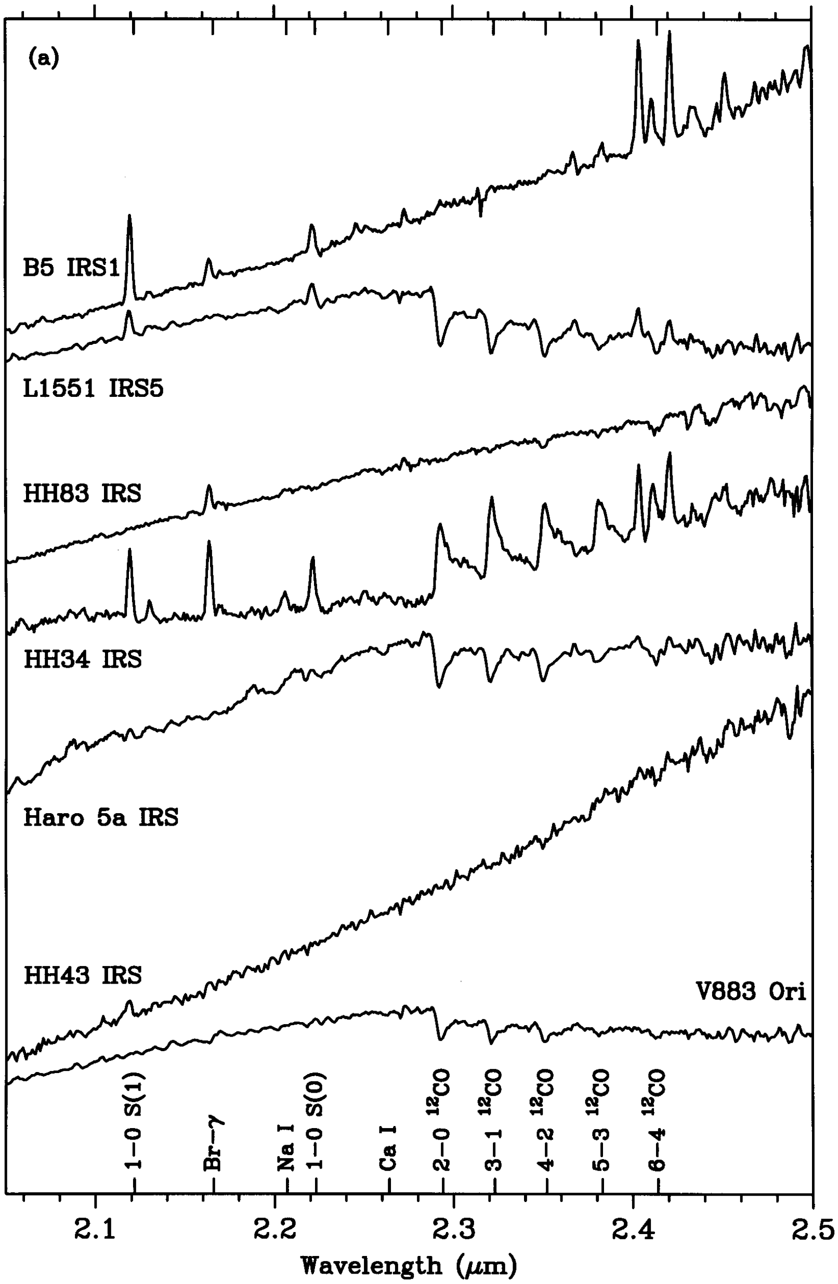

Figure 8: Infrared 2.0–2.5 μm spectra of several HH sources observed with UKIRT.

We have tried to test this hypothesis by observing a sample of embedded HH energy sources, selected so that most of them have rather high luminosities of many dozens to several hundred solar luminosities. If there is a link between HH flows and FUors, we should expect that a much larger fraction of these higher luminosity sources should be caught while they still show FUor characteristics than among the average HH sources. Since a large number of HH sources are optically invisible, the observations should be made in the infrared. We have made 2.0–2.5 μm spectra at UKIRT of 14 HH sources, of which 9 have luminosities higher than the lowest luminosity FUor [16]. Among these 9 sources, 5 show the deep rotationally broadened CO absorption bands characteristic of FUors, while only 1 of the 5 lower luminosity sources shows such bands. It thus appears that the majority of the high luminosity HH sources observed may presently be in elevated FUor states. Figure 8 shows examples of the spectra obtained.

As a star begins to form in the collapse of a dense condensation of gas, a flattened rotating disk soon forms. A vigorous debate is presently taking place among theoreticians about the precise magnetohydrodynamic mechanism that links infall with outflow, but everybody agrees that mass loss is a necessary by-product of the star-formation process, as a star gradually builds up the mass it will have when it eventually reaches the main sequence. HH jets are the visible component of the supersonic mass loss that accompanies the birth of a star, and as such give us indirect information on the very first evolutionary phases of new-born stars.

Acknowledgements

I would like to thank my collaborators Colin Aspin, John Bally, José Cernicharo, Rolf Chini, David Devine, Roland Gredel, Pat Hartigan, Steve Heathcote, Jon Morse, Alex Raga and Luis Felipe Rodríguez for their contributions, which have been essential for the research discussed here, and for enjoyable and stimulating interactions.

References

[1] Heathcote, S., Reipurth, B.: 1992, *AJ* **104**, 2193.
[2] Bally, J., Devine, D.: 1994, *ApJ* **428**, L65.
[3] Reipurth, B., Heathcote, S.: 1991, *AA* **246**, 511.
[4] Heathcote, S., Morse, J., Hartigan, P., Reipurth, B., Schwartz, R.D., Bally, J., Stone, J.: 1996, *AJ* **112**, 1141.
[5] Hartigan, P., Morse, J., Heathcote, S., Cecil, G.: 1993, *ApJ* **414**, L121.
[6] Reipurth, B.: 1989, *Nature* **340**, 42.
[7] Reipurth, B., Raga, A., Heathcote, S.: 1992, *ApJ* **392**, 145.
[8] Gredel, R., Reipurth, B.: 1994, *AA* **289**, L19.
[9] Cernicharo, J., Reipurth, B.: 1996, *ApJ* **460**, L57.
[10] Reipurth, B., Hartigan, P., Heathcote. S., Morse, J., Bally, J.: 1997, *AJ*, in press.
[11] Reipurth, B., Bally, J., Devine, D.: 1997, *AJ*, submitted.
[12] Bally, J., Devine, D., Reipurth, B.: 1996, *ApJ* **473**, L49.
[13] Reipurth, B. Raga, A., Heathcote, S.: 1996, *AA* **311**, 989.
[14] Hartmann, L, Kenyon, S.: 1996, *Annual Review Astron. Astrophys.* **34**, 207.
[15] Dopita, M.A.: 1978, *AA* **63**, 237.
[16] Reipurth, B., Aspin, C.: 1997, *AJ*, submitted.

Bo Reipurth
breipurt@eso.org

A Supernova Found by EROS, Followed with the 1.5-m Danish, and Pictured and Characterised at the 3.6-m Telescope

EROS COLLABORATION

Since 1990, EROS (Expérience de Recherche d'Objets Sombres) has been conducting a search for unseen galactic objects via gravitational microlensing. Our system was upgraded in July 1996 with the installation of the 1-metre Marly telescope in the GPO dome instrumented with two wide-field CCD cameras. The greater part of the observing time is devoted to the search for microlensing events by observing the Magellanic Clouds, the Galactic bulge and the Galactic disk. However, during times when these targets are low in the sky, EROS observes fields at high galactic latitudes in order to search for supernovae at medium redshifts and to measure stellar proper motions. We report here our first supernova discovery (IAU Circular No. 6605).

The new EROS camera consists of two CCD mosaics mounted behind a dichroic cube allowing simultaneous observations in red (750 ± 100 nm) and in visible (560 ± 100 nm) passbands. Each mosaic consists of eight 2048×2048 pixel CCDs and covers a 1.4×0.7 deg^2 field.

We search for supernovae by comparing an image of a given field with a reference image of the same field taken at least one month before. Each observation consists of two 5-minute exposures that are combined to form a ten-minute exposure after identification of cosmic rays. A new image is aligned geometrically and photometrically with the reference image, and the image of superior seeing is processed to match the PSF of the other image. The two images are then subtracted and candidate supernovae are identified in the frame thus obtained. The combined ten-minute exposure makes it possible to identify supernovae up to V = 21.5. The semi-automatic analysis software allows the identification of candidate supernovae during the day following observations.

During the new moon period in March 1997, we searched for supernovae in 8 deg^2 using reference images taken in February. One supernova (SN 1997bl) was found at V = 21.5 in a galaxy of V = 18.5 (see Fig.1).

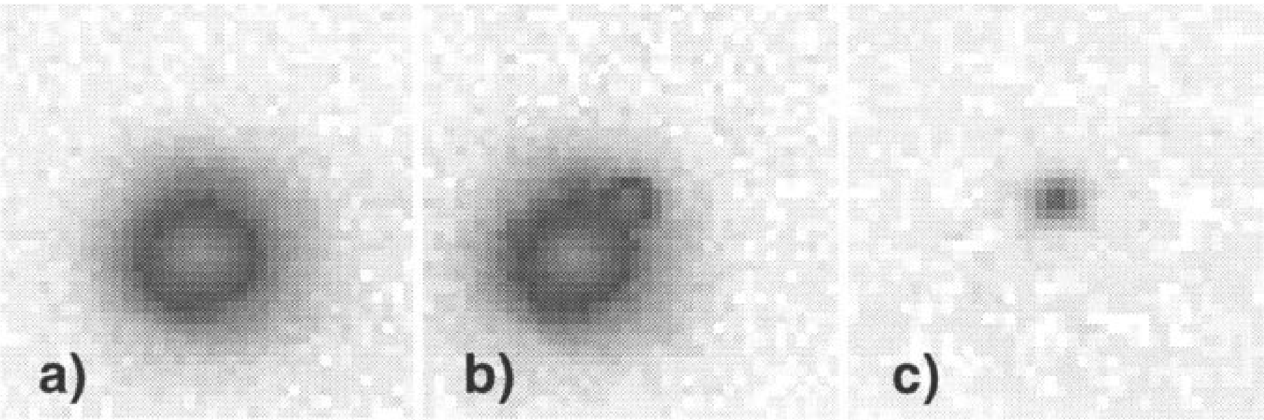

Figure 1: Panel (a) shows the image of the host galaxy, taken on February 3, 1997. Panel (b) shows the image of the host galaxy with the supernova, t ken on March 7, 1997. Panel (c) shows the same image as (b) after subtracting the host galaxy image (a). Note that these images are not matched in seeing.

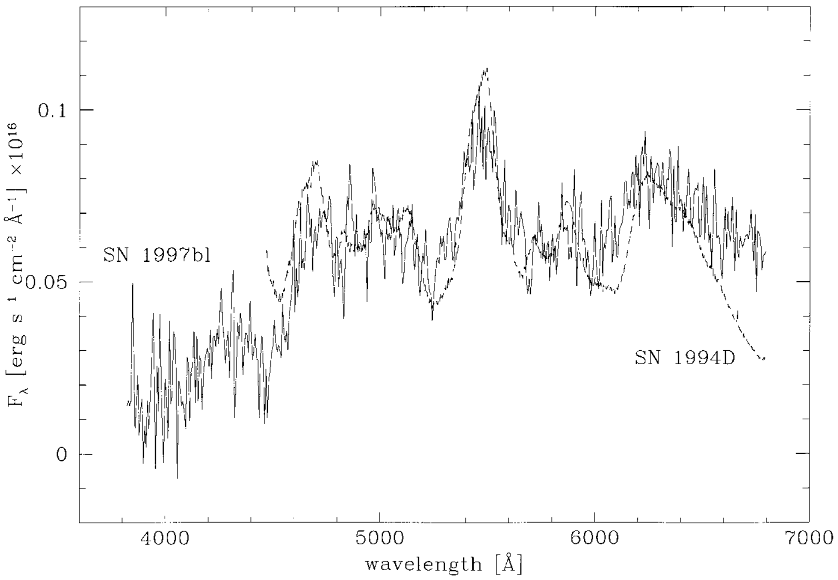

Figure 2: Spectrum of SN 1997bl. Superimposed on the spectrum is that of type Ia supernova SN 1994D 12 days after maximum.

Our requests for follow-up observations using other telescopes at La Silla were warmly received and we thank the observers for their donation of valuable telescope time. Spectra were taken at La Silla with the 3.6-m telescope (Ruiz) and with the 2.2-m (Lehmann). The preliminary reduction of these data identified the supernova as one of type I (IAUC 6605). With a more careful reduction of the 3.6-m data, S. Benetti eventually classified the supernova as type Ia about 10 days after maximum, with the parent galaxy having a redshift of 0.19 (Fig. 2).

Photometric measurements were made with the Danish 1.5-m telescope (Gastro, Tirado and Delfosse). Finally, a superb image using direct imaging was obtained (Benetti and Guisard) at the Cassegrain focus of the 3.6-m telescope (Fig. 3). This is one of the best images produced so far with the 3.6-m and it demonstrates the improvement in image quality accomplished since last year. The image is a 5-minute exposure, the outside seeing was 0.55″ (FWHM) and the seeing measured on the image is 0.65″ (FWHM).

If it is possible to organise a proper follow-up, this programme will develop in a large systematic supernova search. We believe that we can discover supernovae in the range z = 0.05 to 0.2 at the rate of about 1 per two hours observing time, allowing us to obtain a sample of 100 supernovae over a period of 3 years.

Besides being interesting objects in their own right, the value of supernovae as distance indicators useful for cosmological parameter determinations has been demonstrated by previous systematic searches (Hamuy et al.). Two programmes (Leibundgut et al., Kim et al.) are currently searching for supernovae at high redshift ($z \geq 0.3$) with the aim of constraining the deceleration parameter by comparing peak magnitudes with those at lower redshifts.

One of the goals of the EROS supernova programme is to study in detail correlations between SN Ia peak magnitudes with other features of the light curves and spectra. This intermediate-z supernova search will also nicely complement the search for nearby SN which have been and still are the target of intensive studies with ESO-La Silla telescopes, in the framework of a long-term programme, started as ESO Key Programme (Turatto et al., 1990, in *The Messenger* No. 60, p. 15).

At the very moment these lines were written, EROS discovered its second supernova (SN 1997bt, IAUC 6628), at V = 19.5 (see Fig. 4). The host galaxy is classified as number 2915 in the LCRS Survey, with a redshift of 0.06.

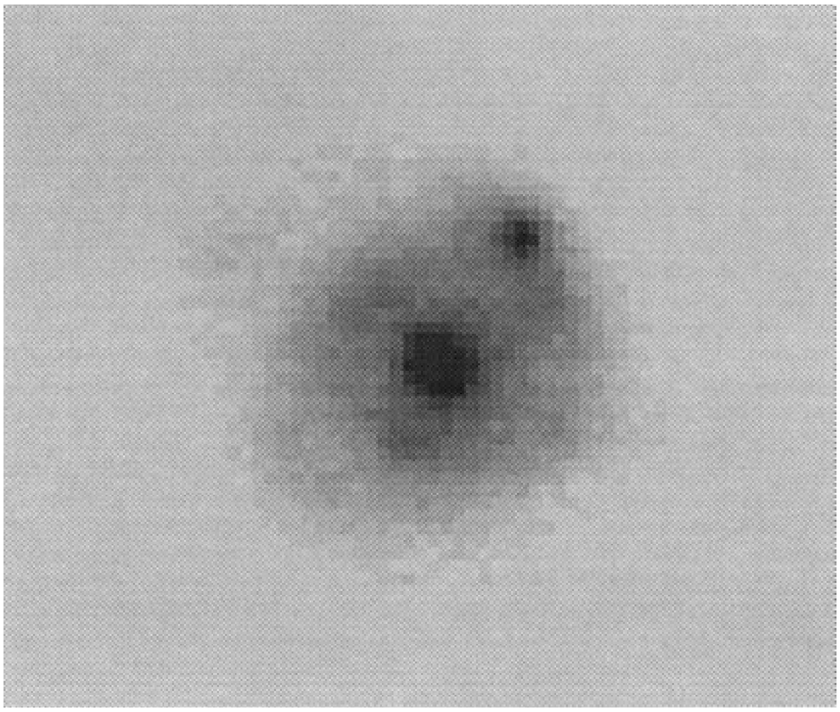

Figure 3: SN 1997bl's host galaxy, as taken by S. Benetti and S. Guisard. The spiral arms can easily be made out, and the supernova clearly stands out from the core of the galaxy.

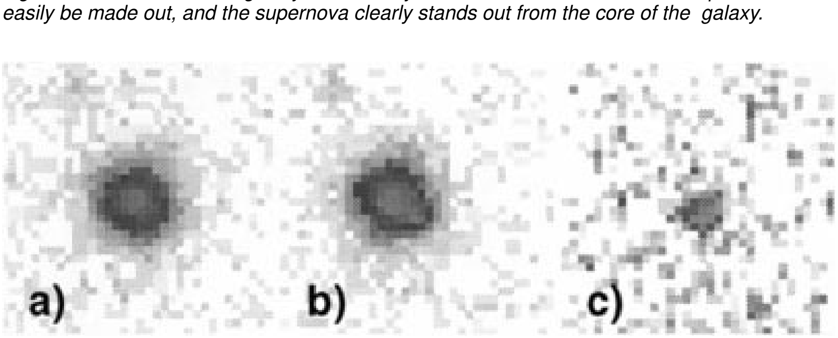

Figure 4: SN 1997bt. Panel (a) shows the image of the host galaxy, taken on February 3, 1997. Panel (b) shows the image of the host galaxy with the supernova, taken on March 31, 1997. Panel (c) shows the same image as (b) after subtracting the host galaxy image (a).

Deconvolution with Correct Sampling

P. MAGAIN[1,*], F. COURBIN[1,2], S. SOHY[1]

[1]Institut d'Astrophysique, Université de Liège, Belgium
[2]URA 173 CNRS-DAEC, Observatoire de Paris-Meudon, France
*Also Maître de Recherches au Fonds National de la Recherche Scientifique (Belgium)

1. Deconvolution

Much effort is presently devoted to the improvement of the spatial resolution of astronomical images, either via the introduction of new observing techniques (as interferometry or adaptive optics) or via a subsequent numerical processing of the image (deconvolution).

In the following, we briefly describe the basic ideas behind a new deconvolution technique which overcomes some of the drawbacks of the traditional methods and which gives results of high photometric and astrometric accuracy. We also show how it can be combined with other techniques (e.g. adaptive optics) to give even better results.

An observed image may usually be mathematically expressed as a convolution of the original light distribution with the "total instrumental profile" – the latter being the image of a point source obtained with the instrument considered, including the atmospheric seeing if the telescope is ground-based. The total blurring function is called the *Point Spread Function* (PSF) of the image.

Thus, the imaging equation may be written:

$$d(\vec{x}) = t(\vec{x}) * f(\vec{x}) + n(\vec{x}) \qquad (1)$$

where $f(\vec{x})$ and $d(\vec{x})$ are the original and observed light distributions, $t(\vec{x})$ is the total PSF and $n(\vec{x})$ the measurement errors *(noise)* affecting the data.

The aim of deconvolution may be stated in the following way: given the observed image $d(\vec{x})$ and the PSF $t(\vec{x})$, recover the original light distribution $f(\vec{x})$. Being an inverse problem, deconvolution is also an ill-posed problem, and no unique solution can be found, especially in the presence of noise. This is due to the fact that many light distributions are, after convolution with the PSF, compatible within the error bars with the observed image. Therefore, regularisation techniques have to be used in order to select a plausible solution amongst the family of possible ones and a large variety of deconvolution methods have been proposed, depending on the way this particular solution is chosen (in

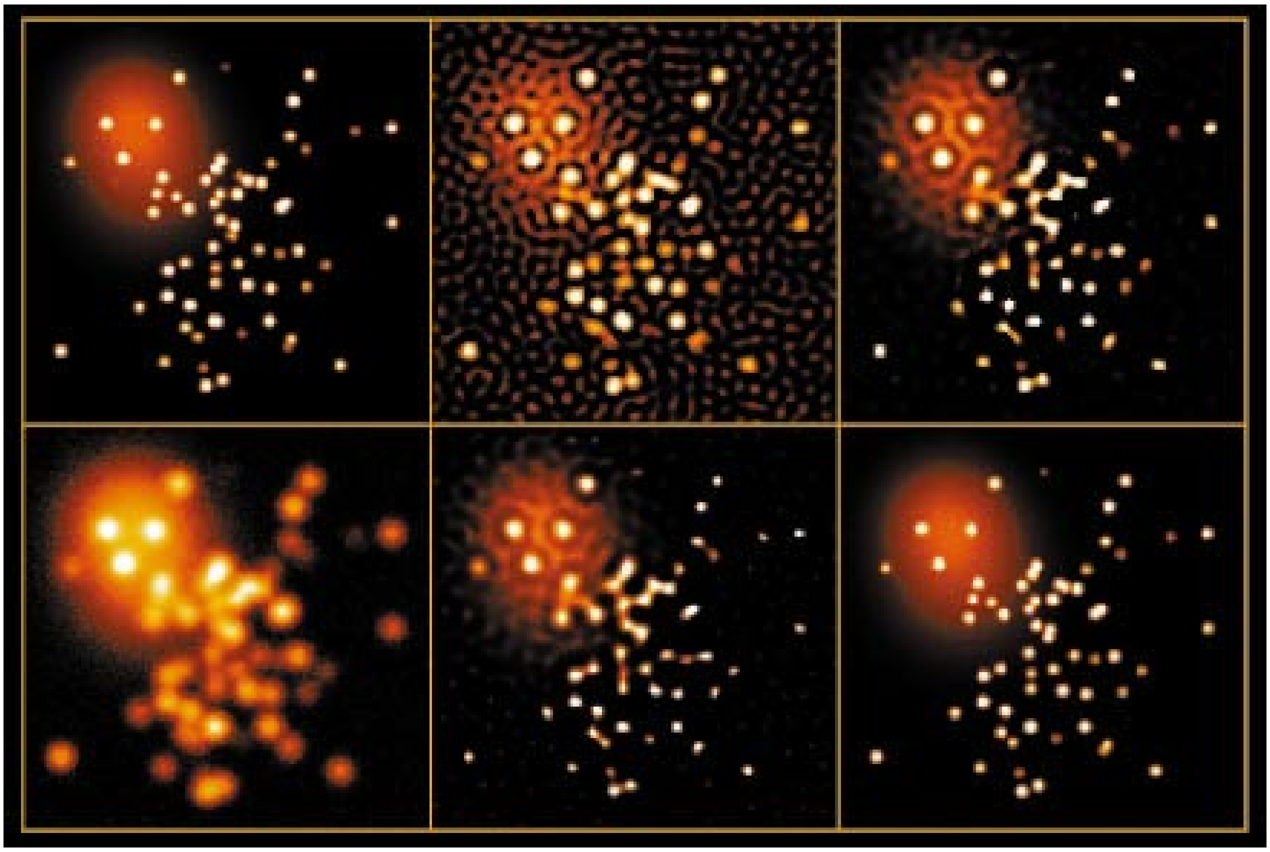

Figure 1: Deconvolution of a simulated image of a star cluster partly superimposed on a background galaxy. Top left: true light distribution with 2 pixels FW M resolution; bottom left: observed image with 6 pixels FWHM and noise; top middle: Wiener filter deconvolution of the observed image; bot om middle: 50 iterations of the accelerated Richardson-Lucy algorithm; top right: maximum entropy deconvolution; bottom right: deconvolution with our new algorithm.

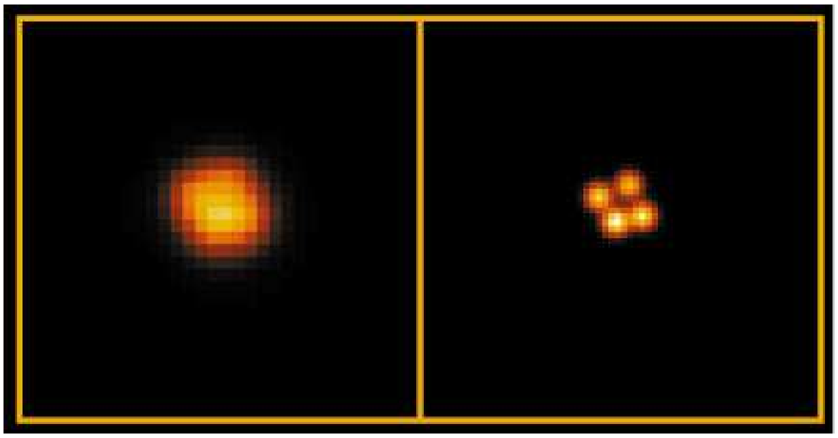

Figure 2: Deconvolution of a pre-discovery image of the Cloverleaf gravitational mirage obtained with the ESO/MPI 2.2-m telescope at La Silla (Chile). Left: observed image with a FWHM resolution of 1.3 arcsec; right: our deconvolution with improved sampling and a FWHM resolution of 0.5 arcsec.

general, the selected solution is the smoothest according to some pre-defined criterion, e.g., the image with the largest entropy).

In order to choose the correct answer in the family of possible solutions to this inverse problem, it is also very useful to consider any available *prior knowledge.* One such prior knowledge is the *positivity* of the light distribution: no negative light flux can be recorded, so that all solutions with negative values may be rejected. The maximum entropy method automatically ensures positivity of the solution. This is also the case, under certain conditions, for other popular methods, such as the Richardson-Lucy iterative algorithm (Richardson, 1972; Lucy, 1974).

However, most of the known deconvolution algorithms suffer from a number of weak points which strongly limit their usefulness. The two most important problems in this respect are the following: (1) traditional deconvolution methods tend to produce artefacts in some instances (e.g. oscillations in the vicinity of image discontinuities, or around point sources superimposed on a smooth background); (2) the relative intensities of different parts of the image (e.g. different stars) are not conserved, thus precluding any photometric measurements. In the following, we identify the main cause of these problems and show how to circumvent it.

2. Sampling

The sampling theorem (Shannon, 1949, Press et al., 1989) determines the maximal sampling interval allowed so that an entire function can be reconstructed from sampled data.

The imaging instruments are generally designed so that the sampling theorem is approximately fulfilled in average observing conditions. A typical sampling encountered is 2 sampling intervals per FWHM of the PSF (this does not ensure good sampling for high S/N images, but is roughly sufficient at low S/N).

The main problem with classical deconvolution algorithms is the following: *if the observed data are sampled so that they just obey the sampling theorem, the deconvolved data will generally violate that same theorem.* Indeed, increasing the resolution means recovering highest Fourier frequencies, so that the correct sampling would become denser.

This is particularly true if the image contains point sources, which is generally the case for astronomical images. Indeed, the angular diameters of most stars ($\ll 0.001$ arcsec) are so small compared to the sampling interval (0.1 arcsec) that they may be considered as point sources ("δ-functions"). In such an instance, it would be hopeless to reduce the sampling interval in an attempt to obtain a good sampling of such "δ-functions".

This is the source of some of the artefacts present in the deconvolved images and, in particular, of the "ringing" around point sources superimposed on a diffuse background. The origin of this "ringing" may be intuitively understood in the following way.

If a point source is located between two sampling points (as will generally be the case), in order to correctly reproduce its position, the deconvolution algorithm will have to distribute its intensity over several sampling points. But, then, the width of the source will be too large and ringing will appear as the algorithm attempts to decrease the intensity on the edges of the reconstructed source, in order to keep the re-convolved model as close as possible to the observed data.

In fact, it is not possible to correctly reproduce both the position and the width of a sampled point source. To reproduce the zero width, the full signal must be concentrated on a single sampling point. On the other hand, to reproduce the position with a precision which is better than the sampling interval, the signal has to be distributed over several points.

3. Solution

The correct approach to this sampling problem is thus *not* to deconvolve with the total PSF $t(\vec{x})$, but rather with a narrower function $s(\vec{x})$ chosen so that the deconvolved image has its own PSF $r(\vec{x})$ compatible with the adopted sampling. These three functions are simply related by:

$$t(\vec{x}) = r(\vec{x}) * s(\vec{x}) \qquad (2)$$

The shape and width of $r(\vec{x})$ can be chosen by the user. The only constraint is that Eq. (2) admits a solution $s(\vec{x})$. The function $s(\vec{x})$ by which the observed image has to be deconvolved is thus obtained as the deconvolution of the total PSF $t(\vec{x})$ by the final PSF $r(\vec{x})$. Of course, the sampling interval of the deconvolved image does not need to be equal to the sampling interval of the

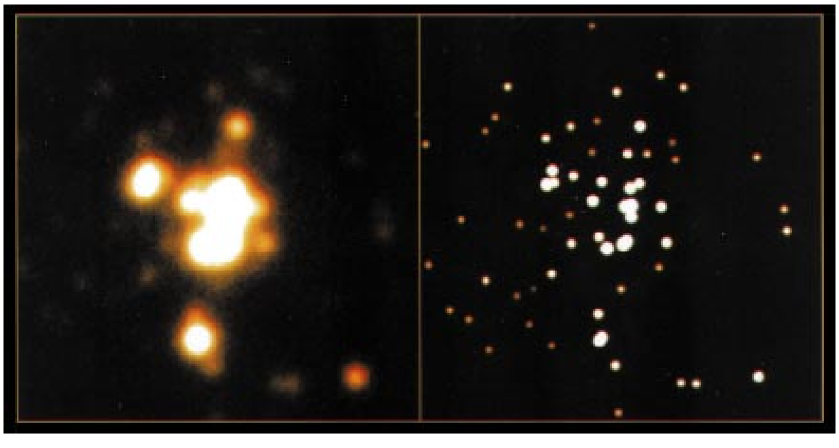

Figure 3: Deconvolution of an image of the compact star cluster Sk 157 in the Small Magellanic Cloud. Left: image obtained with the ESO/MPI 2.2-m telescope at La Silla (1.1 arcsec FWHM); right: deconvolution with our algorithm (0.26 arcsec FWHM).

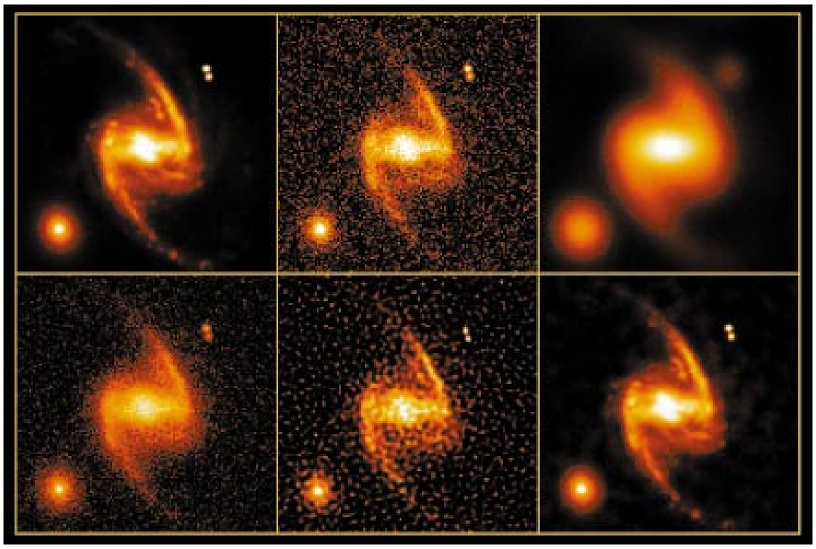

Figure 4: Simultaneous deconvolution of simulated images. Top left: true light distribution with 2 pixels FWHM resolution; top middle: image obtained with a space telescope; top right: image obtained with a large ground-based telescope; bottom left: sum of the two images; bottom middle: simultaneous deconvolution with Lucy's algorithm; bottom right: simultaneous deconvolution with our new algorithm.

original image, so that $r(\vec{x})$ may be much narrower than $t(\vec{x})$, even if the original sampling would not allow it.

Thus, the deconvolution algorithm should not attempt to determine the light distribution as if it were obtained with an *ideal* instrument (e.g. a space telescope with a primary mirror of infinite size). This is forbidden as long as the data are sampled. Rather, the aim of deconvolution should be to determine the light distribution as if it were observed with a *better* instrument (e.g. a 10-m space telescope).

Deconvolution by $s(\vec{x})$ ensures that the solution will not violate the sampling theorem. It also has a very important additional advantage: if the image contains point sources, their shape in the deconvolved image is now precisely known: it is simply $r(\vec{x})$. This is a very strong *prior knowledge,* and it may be used to constrain the solution $f(\vec{x})$, which can be written as the sum of smooth background plus a number of point sources, whose intensities and positions are unknown.

Another prior knowledge can be used to constrain the solution: indeed, the background itself should not contain any Fourier component with frequency higher than allowed by the final deconvolved PSF $r(\vec{x})$, and this knowledge can be used to force smoothness on the scale length of $r(\vec{x})$.

4. Examples

Figure 1 compares the results of our new deconvolution algorithm to those of three classical methods in the case of a simulated star cluster partly superimposed on a smooth background (e.g. a

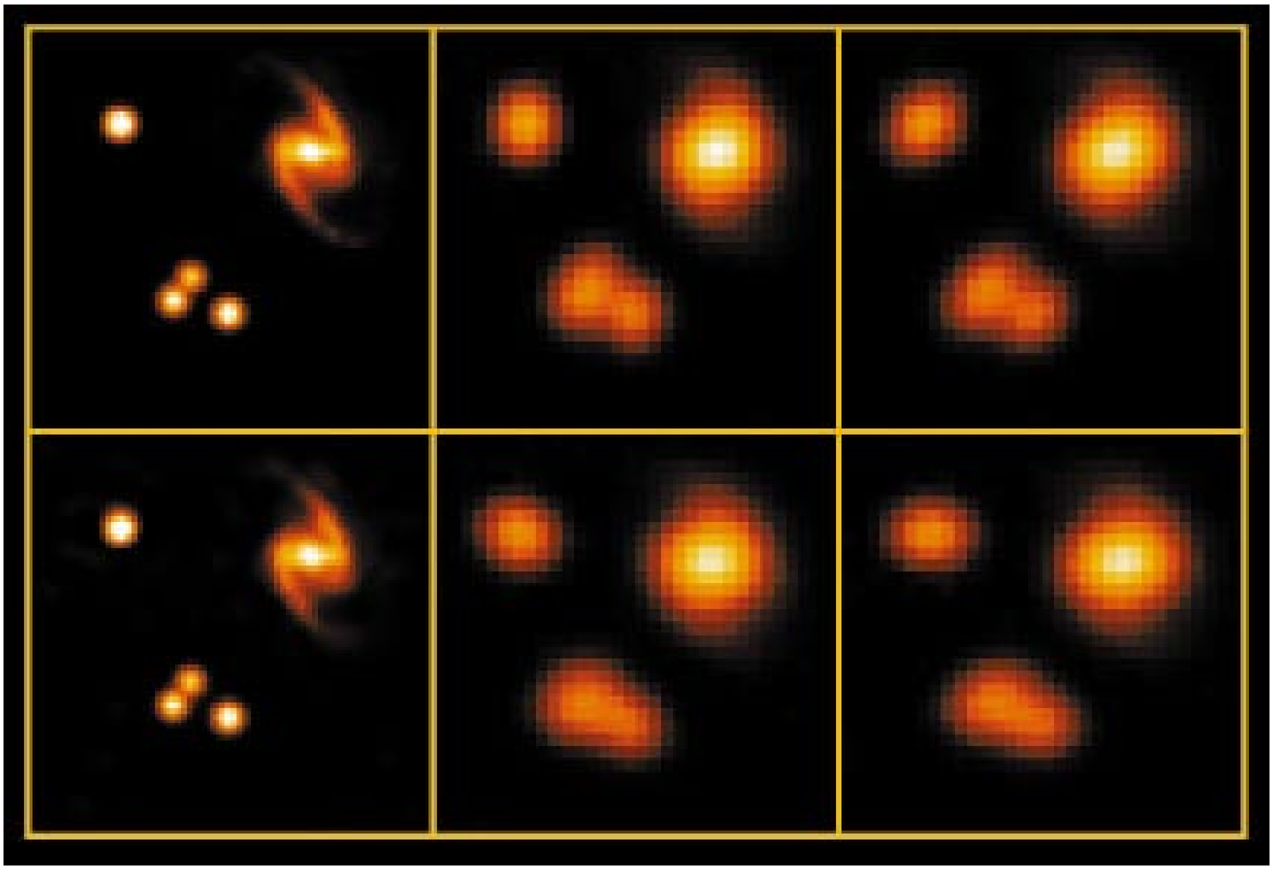

Figure 5: Simultaneous deconvolution of 4 simulated adaptive-optics-like images. Top left: true light distribution with 2 pixels FWHM resolution; middle and right 4 images obtained with the same instrument but in varying atmospheric conditions; bottom left: simultaneous deconvolution with our new algorithm.

distant elliptical galaxy). It is clear that our result is free from the artefacts present in the other methods and that it allows an accurate reconstruction of the original light distribution.

An application to real astronomical data is shown on Figure 2, which displays a mediocre-resolution image of the "Cloverleaf", a gravitationally lensed quasar (Magain et al., 1988), together with the deconvolved version, using a sampling interval twice as short. The four lensed images, which were unresolved in the original data, are completely separated after deconvolution. The deduced fluxes are fully compatible with those measured on higher-resolution images and, although the original resolution is 1.3 arcsec only and the pixel size is 0.35 arcsec, the deduced image positions are accurate to 0.01 arcsec.

Figure 3 illustrates the deconvolution of an image of the compact star cluster Sk 157 in the Small Magellanic Cloud (Heydari-Malayeri et al., 1989). The original image was obtained with the ESO/MPI 2.2-m telescope at La Silla, in average seeing conditions (1.1 arcsec FWHM). While the original maximum entropy deconvolution (Heydari-Malayeri et al., 1989) allowed to resolve the cluster into 12 components, our new algorithm detects more than 40 stars in the same area.

Another important application of our algorithm is the simultaneous deconvolution of different images of the same field. These images may be obtained with the same instrument or with different ones. The solution is then a light distribution which is compatible with all the images considered. Our technique even allows to let, e.g., the intensities of the point sources converge to different values in the different images, so that variable objects may be considered. This should be very useful for the photometric monitoring of variable objects in crowded fields (e.g. Cepheids in distant galaxies).

Figure 4 illustrates this simultaneous deconvolution on simulated images, the first of which has a good resolution but a poor S/N (as might be obtained with a space telescope) and the second one a low-resolution and a high S/N (a typical image from a large ground-based telescope). Contrary to Lucy's method (Lucy, 1991) which is very sensitive to the noise present in one of the images, our technique allows to reliably recover both the high resolution of the space image and the hidden information content of the ground-based one.

In the same spirit, our algorithm is well adapted to the processing of images obtained with adaptive optics techniques. In the latter, numerous short exposures of the same field are usually obtained, the shape of the mirror being continuously adapted to correct for atmospheric distortions. So, the observations consist in a number of images of the same field, each of them having its own PSF. Performing a simple sum results in an image whose spatial resolution is typical of the average observing conditions, while a simultaneous deconvolution not only allows to take count of the best conditions, but even results in an improved resolution by optimally combining the information content of the different images. A simple illustration of these considerations is provided by Figure 5, which shows the simultaneous deconvolution of four adaptive-optics-like images of the same field, where the PSF as well as the image centring vary from one observation to the other.

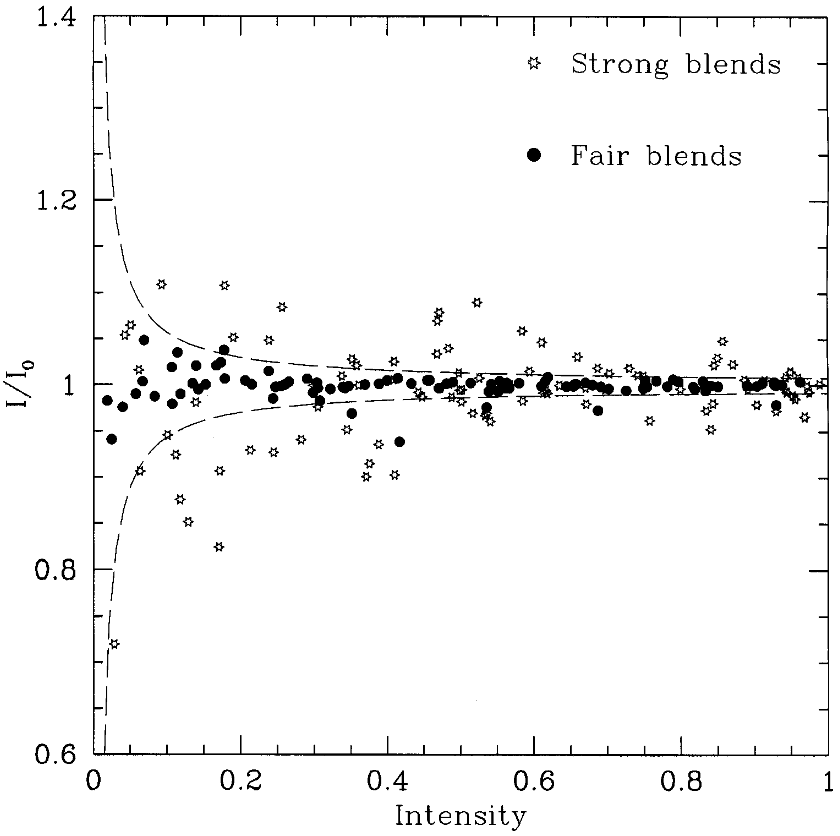

Figure 6: Photometric test performed on a synthetic field containing 200 stars with random positions and intensities, nearly all blended to various degrees. The relative errors are plotted against the total intensity (the latter being on an arbitrary scale, corresponding to an integrated S/N varying from 10 to 400). Open symbols represent heavily blended stars (the distance to the nearest neighbour is smaller than the FWHM), filled symbols correspond to less blended objects. The dashed curves are the theoretical 3σ errors for isolated stars, taking into account the photon noise alone.

Traditional deconvolution methods are notoriously unable to give photometrically accurate results. The main reasons are that (1) the rings which tend to be produced around point sources may interfere with neighbouring objects so that the flux is redistributed between the sources and (2) the smoothing recipe generally forces the stars to deviate as little as possible from the background, so that the intensity peaks are generally underestimated.

Our algorithm naturally avoids these two biases, as is illustrated in Figure 6, which shows the results of a photometric test applied to a synthetic field containing 200 stars in a 128×128 pixels image, nearly all the stars being blended to various degrees (197 stars out of 200 have the nearest neighbour within 2 FWHMs). Moreover, these stars are superimposed on a variable background. Figure 6 clearly shows that no systematic error is present, and that the intensities of all but the most severely blended objects are reproduced with errors compatible with the photon noise.

More details about the deconvolution technique and astronomical applications can be found at: http://vela.astro.ulg.ac.be/imaproc

References

Heydari-Malayeri, M., Magain, P., Remy, M. *Astron. Astrophys.* **222**, 41 (1989).
Lucy, L. *Astron. J.* **79**, 745 (1974).
Lucy, L. *ST-ECF Newsletter* **16**, 6 (1991).
Magain, P., Surdej, J., Swings, J.-P. et al. *Nature* **334**, 325 (1988).
Press, W.H., Flannery, B.P., Teukolsky, S.A. & Vetterling, W.T. *Numerical Recipes* (Cambridge University Press, 1989).
Richardson, W.H. *J. Opt. Soc. America* **62**, 55 (1972).
Shannon, C.J. *Proc. I.R.E.* **37**, 10 (1949).

P. Magain, F. Courbin
magain@astro.ulg.ac.be
courbin@astro.ulg.ac.be

High-Resolution Imaging with Bad Seeing: PKS 1610-771 as a Test Case

F. COURBIN [1,2], J.-F. CLAESKENS[1,]*

[1] Institut d'Astrophysique, Université de Liège, Belgium; [2] URA 173 CNRS-DAEC, Observatoire de Paris-Meudon
**Also Aspirant au Fonds National de la Recherche Scientifique, Belgium*

1. Introduction

In a previous issue of *The Messenger* (Courbin et al., 1996), we presented NTT subarcsecond images of the luminous quasar PKS 1610-771, together with its spectrum. The analysis of the data (see also Courbin et al., 1997) leads to the plausible conclusion that the quasar is heavily obscured by dust.

PKS 1610-771 has recently been observed in the infrared, but under much poorer seeing conditions (final frame with a FWHM of 1.66″). We use these data to derive the infrared photometry of the quasar and also to detect the IR counterparts of the faint fuzzy objects surrounding the QSO, which were originally discovered in the optical. This is achieved by using the new deconvolution and co-addition algorithm developed by Magain et al. (1997a, b) to combine 6 individual *K′* images.

Since the high-resolution optical images of PKS 1610-771 can provide a check of the co-addition results, we use these data as an example to present a new way of improving spatial resolution, based on the simultaneous deconvolution of several images of the same field.

2. Observations – Reduction

The highly luminous quasar PKS 1610-771 was imaged in the infrared *K′* band during the night of the 19th to 20th of August 1996, with IRAC2b, mounted at the f/35 adapter at the 2.2-m ESO/MPI telescope on La Silla. Lens LB was used. The corresponding pixel size projected on the sky is 0.278″, and the field size is 71″.

The airmass of the object in the middle of the exposure was high (1.6), and the observing conditions were rather poor (average seeing of 1.66″, and fast variations of the background). Since the target is not much extended, and since the field is not crowded, small (7″) telescope offsets were done between each individual exposure in order to subtract the background. Special attention was paid in order to maintain simultaneously in the field, the quasar together with a nearby bright star, used to determine the Point Spread Function (PSF).

The total exposure time amounts to 540 seconds, and the calibration of the zero point was done by observing the infrared standard star HD 29250 (Van der Bliek et al., 1996).

3. Image Co-addition

The IR data consist of 6 individual exposures that need to be optimally combined and sharpened. This can be done in classical ways, just by aligning and averaging the 6 frames. However, a much more efficient method is to deconvolve the images simultaneously. The aim of the process is to find the best deconvolved model, compatible with each of the 6 frames, i.e. within the error bars fixed by the photon noise of each image.

A PSF has to be calculated in order to carry out the deconvolution. Fortunately, a suitable reference star (i.e. comparable in brightness to the QSO) is present on each frame. The good sampling of the data (FWHM 6 pixels) allows the construction of an accurate PSF. Even if the data are well sampled, Magain et al. (1997a, b) show that deconvolving by the total PSF of the image results in a violation of the sampling theorem and produces the so-called "deconvolution artifacts". In order to avoid this problem, a narrower PSF has to be used. This ensures that the sampling of the deconvolved image is always compatible with all the spatial frequencies it contains. This has two consequences: (1) the shape of the final deconvolved stars is known and (2) one image can be decomposed in a sum of point sources, plus a (deconvolved) diffuse background. In addition, there is no reason for the pixel size of the deconvolved frame to be the same as in the data. This is of particular interest in the case of IR data where numerous dithered frames are usually taken. In order to take full advantage of the dithering between the exposures, we use for the deconvolution a pixel size two times smaller than in the original data. Our final linear pixel size is then 0.278″/2 = 0.139″. We *choose* the final "deconvolved" PSFs as Gaussians with a FWHM of 6 (small) pixels or, equivalently, we *choose* a final "seeing" of 0.83″. This choice allows to compare the results with our NTT *R*-band images which have a seeing of 0.85″. There is in fact no formal limitation to the final resolution, as soon as the sampling of the deconvolved image remains within the limits imposed by the sampling theorem. It is however our experience that low S/N data do not really allow a deconvolution by much more than a factor 2. Once the final FWHM for the deconvolved image is chosen, the nearby star is used to generate the PSF actually needed for the deconvolution process.

In practice, one has to estimate *guess* starting conditions in order to run the deconvolution code. The background component of the model image is initially set to zero. From NTT images, we know that there are 2 point sources in the field considered here. This is the only prior knowledge we use. Guess intensities and centre positions are supplied for these two objects, in each of the six images.

The programme finds the optimal geometrical transformation between the images during the deconvolution process; therefore, no prior alignment of the frames has to be performed. Since each of the 6 frames is considered with its own (narrower) PSF and since the minimisation procedure takes into account the photon noise of each of the 6 images, the result is an optimal combination (with improved seeing and sampling) of the individual data. Both the seeing and S/N ratio of the images are in fact automatically used to weight the individual frames. In addition, the negative pixel values introduced by the background subtraction necessary in the IR, are not set to zero as needed to run traditional deconvolution algorithms; no positivity constraint is necessary. In fact, the data frames are never changed or interpolated, at any moment of the calculation.

The deconvolution procedure minimises the χ^2 between the re-convolved model and the whole data set, with the further constraint that the background part of the deconvolved image is smooth on the length scale of the deconvolved PSF (the one chosen by the user). The solution is considered acceptable only when the 6 residual frames (corresponding to the 6 data frames), in units of the photon noise, show over the whole field a correct statistical distribution, i.e. Gaussian with a zero mean and a standard deviation of 1. The outputs of the procedure are a deconvolved image and a deconvolved background, free of any contamination by the point sources. As an interesting by-product of the programme, the peak intensities and the positions of the point sources are also returned.

4. Results – Discussion

The simultaneous deconvolution of our 6 frames yields the images displayed in Figure 1 (panels (2) and (3)).

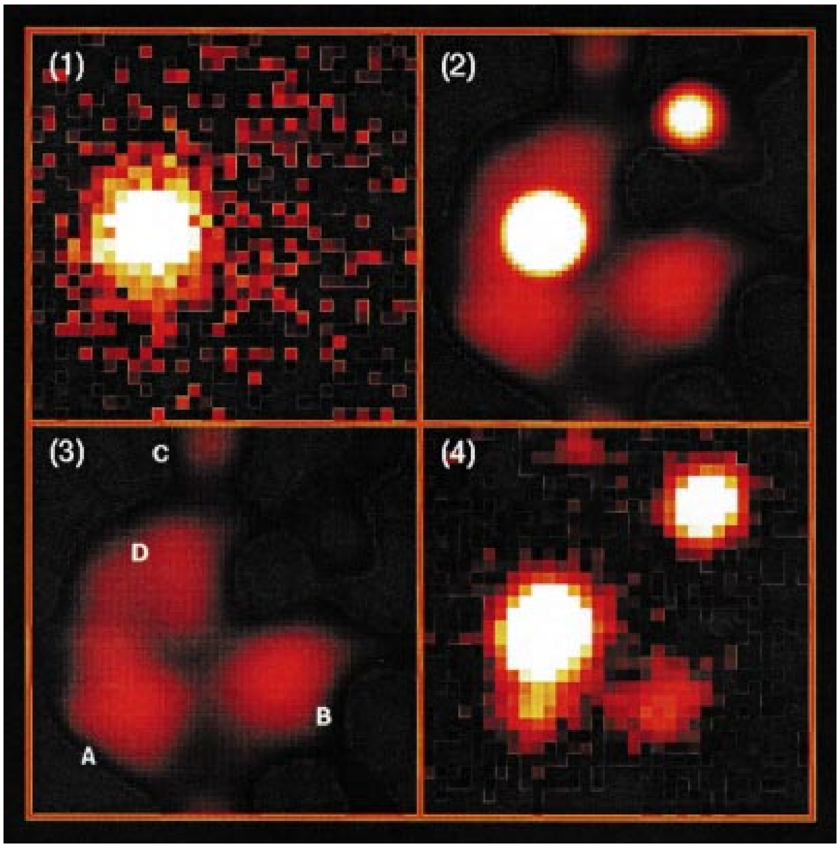

*Figure 1: Comparison of the IR results with high-resolution optical data: field of 6″ × 6″ showing PKS 1610-771. (**1**) Stack of the 6 K′ band images. The seeing is 1.66″. (**2**) Simultaneous deconvolution of the 6 frames. While the original pixel size is 0.278″, it is now 0.139″ and the final FWHM of the deconvolved point sources is 0.83″. (**3**) Deconvolved background showing the faint fuzzy objects hidden by the QSO's light. (**4**) High-resolution R-band NTT image with a seeing of 0.85″ (pixel size of 0.268″), for direct comparison with the IR deconvolved image. Note that the low light levels are fully displayed in all four images, so that any deconvolution artifact would appear, if present.*

The final seeing of our deconvolved IR image is close to the seeing of a reference *R*-band image taken with the NTT +EMMI. It is clear from Figure 1 that objects A, B and C are real: they can be seen on the NTT image. Object D is also real, it appears on the NTT frame after a PSF is subtracted from the QSO's image (see Courbin et al., 1996 and 1997).

From the peak intensities of the point sources, we get the relative photometry of the QSO and the star present in the field. Since the algorithm preserves flux, absolute aperture photometry can be directly performed on the deconvolved image. The *K′* magnitude of the QSO has been independently estimated on the original and deconvolved frames. The two measurements are fully compatible. The deconvolved background is used (panel (3) in Fig. 1) in order to estimate the IR magnitudes of objects A, B, C and D. We have taken the *R* magnitudes from Courbin et al. (1997) to derive the $R - K'$ colour for each object (see Table 1).

Table 1: Estimated K′ magnitudes and R-K′ colours

Object	K′	R-K′
PKS 1610-771	15.1 ± 0.1	3.1 ± 0.25
STAR	18.1 ± 0.3	1.5 ± 0.35
Gal A	17.8 ± 0.5	3.5 ± 0.60
Gal B	17.9 ± 0.5	3.4 ± 0.60
Gal C	20.0 ± 0.5	3.0 ± 0.60
Gal D	18.3 ± 0.5	4.7 ± 0.60
PSF star	14.9 ± 0.1	1.8 ± 0.10

Particular attention has to be paid to the influence of noise on the quality of the deconvolved image. Indeed, in spite of its perfect noise-free aspect, one has to remember that the model is reconstructed from imperfect data. Therefore, the photometry derived from this frame is affected by photon noise, as are the original data. The error bars given in Table 1 are estimated from the integrated photon noise in each object. In addition, we used as a prior knowledge the fact that the QSO and its nearby star companion are point sources. The deconvolution process allows to confirm the QSO as a point source (from the residual frames), but the signal-to-noise ratio in the nearby star image is too low to draw definite conclusions about its precise shape. Star/galaxy discrimination requires better S/N. However, we also performed the deconvolution with only one point source included in the fit (for the QSO). From the resulting deconvolved image, we derive for the star the same $R - K'$ colour than with the former deconvolution.

PKS 1610-771 has a $R - K'$ colour index of 3.1. Using the photographic magnitude from Hunstead and Murdoch (1980), its $B - K'$ is at least 3.8, supporting the hypothesis of strong reddening by dust (Webster et al., 1995). Intrinsic photometric variation of the QSO between the different observations cannot be ruled out, although variations of more than one magnitude would be necessary to significantly change its red colour.

The 4 fuzzy objects close to the QSO have a red $R - K'$ colour index which confirms that they are galaxies. Comparison of the apparent magnitudes and colours of objects A, B and D, with predictions from galaxy evolution models (Pozzetti et al., 1996), leads to the conclusion that they are more likely foreground elliptical galaxies at a redshift between 0.5 and 1.0. Spirals would have been fainter or bluer, at any redshift. Only object C is compatible with a spiral galaxy at $z > 1$.

These data have allowed the determination of the K′ magnitude of PKS 1610-771. The deconvolution process made possible the study of its 4 nearby fuzzy companions, in spite of the rather bad seeing of the IR observations. We have used PKS 1610-771 as a test case because high-resolution images of the object were available to check the validity of a new deconvolution process. We show that relatively good spatial resolution can be achieved even under poor seeing conditions, still keeping the photometric and astrometric properties of the data. The only conditions required for the success of the method are: (1) a good sampling of the original data, (2) a good knowledge of the PSF (which also has to be stable across the field).

References

Courbin F., Hutsemékers D., Meylan G., Magain P., Djorgovski S.G., 1996, *The Messenger* No. **85**, p. 27.

Courbin F., Hutsemékers D., Meylan G., Magain P., Djorgovski S.G., 1997, *A&A*, **307**, 656.

Hunstead R. W., Murdoch, H. S., 1980, *MNRAS*, **192**, 31 p.

Magain P., Courbin F., Sohy S., 1997a, *The Messenger*, present issue.

Magain P., Courbin F., Sohy S., 1997b, *ApJ*, submitted.

Pozzetti L., Bruzual A.G., Zamorani G., 1996, *MNRAS* **281**, 953.

Van der Bliek N.S., Manfroid J., Bouchet P., 1996, *AAS* **119**, 547.

Webster R.L., Francis P.J., Peterson B.A., Drinkwater M.J., Masci F.J., 1995, *Nature*, **375**, 469.

F. Courbin
courbin@astra.astro.ulg.ac.be

ANNOUNCEMENTS

Mirror of NOAO IRAF Archive Now Available at ST–ECF/ESO

R. HOOK

The IRAF system and its layered software packages such as STSDAS and PROS are now widely used within ESO and at other astronomical sites around Europe. When new versions of such packages are required, or up-to-date documentation about the current ones needs to be consulted, it is normally necessary to contact NOAO in Tucson or access the Web pages there.

In order to make access to this information easier for local ESO users and European users in general, a “mirror” of the NOAO IRAF ftp directory tree, including all the Web pages, has been established at the ST–ECF at ESO-Garching. This mirror is automatically updated each night to keep it identical to the Tucson version. This means that the latest information about IRAF will be available at the ST–ECF within a day of the changes being made in Tucson and can be accessed directly over fast internal network connections for Garching users, over the ESO link from Chile or using European networks.

The Web pages which contain most of the information of interest to users can be accessed at http://ecf.hq.eso.org/iraf/web. The IRAF ftp archive, which contains the software distributions for many platforms and also many layered products, is available at http://ecf.hq.eso.org/iraf/ftp or via anonymous FTP at ftp://ecf.hq.eso.org/iraf.

Another mirror has already been established at the Rutherford Laboratory in England and been found very useful. We hope that the ECF one will also be of help. I am very grateful for help and encouragement from Mike Fitzpatrick (NOAO) and Dave Terrett (RAL) who did most of the work the first time around when they set up the RAL mirror.

ESO Imaging Survey: Update

L. DA COSTA

We are pleased to inform that the OPC, following the recommendation of the ESO Imaging Survey Working Group, has approved the revised version of the project in its entirety. This revised version emerged after meetings of the Working Group in early March and late April. The approved observing strategy is as follows:

EIS-WIDE:

It will cover four separate fields of six square degrees each, distributed in right ascension over the interval 22^h to 10^h. All these fields will be observed in two passbands (V_w 24.2, I_w 23.2) and will serve primarily for the search of distant clusters. The field centred near the SGP will also be observed in the B_w passband (B_w 24.3) and in U' (U' 24) over a smaller area (1.9 square degrees) using SUSI2. Besides the search for clusters, this field will be used to provide close lines of sight to relatively bright high-z QSOs (z 1.7) that can be used to study the three-dimensional distribution of absorption-line systems with UVES. It will also provide 100 QSOs at z 3.

EIS-DEEP:

The deep observations have been divided into two parts: DEEP-I will consist of deep images in four optical (U', Gunn-g, Gunn-r, I to 26) and two IR bands (J 24, K' 21.5) of a single SUSI2/SOFI field with the primary goal of finding galaxies in the redshift interval 1 z 4 and provide targets for ISAAC and FORS in the first semester of 1999; DEEP-II will consist of deep optical/infrared exposures over nine SUSI2/SOFI fields, including the HST-HDFS field to the same limiting magnitude as Deep-I. The aim is to provide high-redshift galaxy candidates for studies of galaxy evolution and clustering at high-redshift.

We note that the co-ordinates for some fields are still tentative as it is the HDFS. For more information and regular updates see the WWW EIS page.

ESO IMAGING SURVEY

Survey	Co-ordinates	Filters	Notes
WIDE	22^h42^m – 39°28′	V_w, I_w	
	00^h51^m – 28°54′	U', B_w, V_w, I_w	
	05^h38^m – 23°51′	V_w, I_w	
	09^h48^m – 20°00′	V_w, I_w	TBC
DEEP-I	09^h48^m – 20°00′	U', Gunn-g,Gunn-r, I, J, K'	TBC
DEEP-II	22^h33^m – 60°33′	U', Gunn-g,Gunn-r,I, K'	TBC

Joint ESO/AUSTRALIA Workshop

LOOKING DEEP IN THE SOUTHERN SKY

Sydney 10–12 December 1997

A number of exciting new facilities will soon be available in the southern hemisphere: in the optical, the VLT is expected to begin operations in mid-1998, in the radio the Australia Telescope Compact Array will be upgraded to higher frequencies (22 and 90 GHz) together with an improvement of the VLBI facilities. Moreover, new deep surveys are underway or proposed for the southern hemisphere: these inc ude the southern Hubble Deep Field, the ESO Imaging Survey (EIS), panoramic deep surveys with the UK Schmidt telescope, and the AAT 2dF galaxy/QSO redshift survey in the optical; the Parkes multi-beam HI survey and MOST Wide Field continuum survey at radio wavelengths.

The ge eration of large databases, and the opportunity for sensitive follow-up observations in a complementary waveband, mean that co-ordinated radio and optical projects in the southern hemisphere are likely to become increasingly attractive and important.

The a m of this workshop is to bring together people interested in discussing the impact of all these new facilities on extragalactic astronom and to provide a focus for stimulating new co-ordinated projects between (mainly but not only!) radio and optical astronomers. The workshop will address a wide range of scientific topics relevant to deep radio and optical surveys in the southern hemisphere. The main areas to be covered are:

(1) COSMOLOGY AND LARGE-SCALE STRUCTURE: cosmological parameters from redshift surveys and supernovae, large-scale structure in the local and distant universe, gravitational lensing, cosmological tests from the new surveys

(2) OBJECT SEARCHES: how survey combinations and particular survey techniques work to find particular object classes

(3) THE HIGH-REDSHIFT UNIVERSE: strategies for selecting high-z objects, clusters at $z>1$, the field galaxy population at high redshift, gas and dust at high redshift, high-redshift radio galaxies and QSOs

(4) THE LOCAL UNIVERSE: the faint blue population and its evolution, faint radio source population, HI in the local universe, links between AGN and starbursts

Scientific Organising Committee

B. Boyle (AAO), R. Cannon (AAO), M. Colless (MSSSO), L. Da Costa (ESO), W. Couch (UNSW), S. D’Odorico (ESO), J. Danziger (ESO), R. Ekers (ATNF), W. Freudling (ST-ECF), R. Fosbury (ST-ECF, co-Chair), I. Hook (ESO), R. Morganti (ATNF/IRA, co-Chair), E. Sadler (Univ. Sydney)

Contact Addresses:

R. Morganti, ATNF,
PO Box 76, Epping NSW 2121, Australia

R.A. Fosbury, ST-ECF/ESO, Karl-Schwarzschild-Str. 2,
D-85748 Garching bei München, Germany

By the time the present issue of *The Messenger* is out, the internal workshop described below will have taken place at ESO. An extensive summary of the workshop will appear in a forthcoming issue.

ESO Internal Workshop on Forecasting Astronomical Observing Conditions

Garching, 29–30 May, 1997

Summary

It is now understood that most future ground-based observatories will make use of flexible scheduling tools to select the observing mode best adapted to the observing conditions.

ESO has been conducting a wide survey of existing and potential forecasting techniques, and several feasibility studies are close to completion. It is thus time to prepare the specifications of the operational tools and services to be developed for the VLT.

Note: information is also available on the WEB at: ftp://dimm2.hq.eso.org/public_html/seminar/predict/agenda.html

Preliminary Agenda:

SESSION I: STATISTICAL METHODS

• "Performance analysis of multivariate and Neural Network methods for the prediction of Temperature and Seeing at Astronomical Observatories" (M. Sarazin, ESO)
• "The VLT Enclosure and Mirror Temperature Control System: Methodology and Operational Developments" (L. Noethe, ESO)

SESSION II: SATELLITE IMAGERY

• "Evaluation of Satellite Derived Precipitable Water Vapour Measurements – a Comparison with Antofagasta Radiosonde and Paranal Ground PWV Monitor Measurements" (A. Erasmus, U. of Northern Colorado)
• "Development and Evaluation of an Improved Methodology for Forecasting Cirrus Cloud Cover and PWV above Paranal and La Silla" (A. Erasmus, U. of Northern Colorado)

SESSION III: NUMERICAL MODELLING

• "Comparison of ECMWF and ESO database over the period 89–93" (R. Deidda, CRS4 Cagliari)
• "Results of a Limited Area Model on Some Test Cases" (Pr. A. Speranza, CRS4 Cagliari)
• "Post-processing ECMWF forecast – Kalman Filtering Results at Paranal " (M. Maroccu, CRS4 Cagliari)
• "The basis for predicting optical turbulence from mesoscale meteorological modelling" (J. Vernin, U. of Nice)
• "Modelling optical turbulence over Paranal with Meso-nh: the first results" (E. Masciadri, U. of Nice)

SESSION IV: OPERATIONAL FORECAST SYSTEMS

• "The ECMWF data assimilation and operational forecast scheme: a user guide" (K. Fielding, ECMWF Reading, to be confirmed)
• "Proposal for a system of operational forecast finalised to meteorological prediction for ESO observatories in Chile" (Pr. A. Speranza, CRS4 Cagliari)
* "Proposal for an operational forecast of cloud cover and precipitable water vapour over ESO observatories in Chile" (A. Erasmus, U. of Northern Colorado)

SESSION V: DISCUSSION

FIRST ANNOUNCEMENT

ESO/OSA Topical Meeting

"Astronomy with Adaptive Optics – Present Results and Future Programs"

September 11–17, 1998
Garching bei München, Germany

For more information on this meeting, please consult the ESO Web pages at http://www.eso.org/aot . There will be the electronic subscription forms, as well as travel/lodging information/reservation, and paper preparation instructions.
Otherwise e-mail at ezuffane@eso.org

PERSONNEL MOVEMENTS

International Staff (1 April – 30 June 1997

ARRIVALS

EUROPE

KROKER, Harald (D), Fellow
KÜRSTER, Martin (D), Astronomer
WIDL, Alfred (D), Accounting Clerk
BENNER, Jens (D), Student
PIRZKAL, Norbert (F), Scientific Systems Analyst/Programmer
PRIMAS, Francesca (I), Fellow

CHILE

PIZZELLA, Alessandro (I), Fellow

DEPARTURES

EUROPE

ADORF, Hans-Martin (D), Scientific Systems Analyst/Programmer
FORSTMANN, Pierre (F), Software Engineer
BÄUMER, Volker (D), Student
MANIL, Emmanuel (F), System Engineer
ANDERSEN, Torben (DK), Senior Systems Analyst

CHILE

BOUCHET, Patrice (F), Infrared Astronomer
REIPURTH, Bo (DK), Astronomer

Local Staff (1 April – 30 June 1997)

ARRIVALS

BAUERLE, Mary (RCH), Executive Bilingual Secretary
URRUTIA, Christián (RCH), Human Interface Programmer
CARVAJAL, Alfredo (RCH), Procurement Officer
VALDÉS, Rafael (RCH), Instruments Operator
DE CASTRO, Rodrigo (RCH), Public Relations Officer
KIEKEBUSCH, Mario (RCH), Informatics Engineer
BUGUEÑO, Erich (RCH), Senior Mechan. Technician
OSORIO, Juan (RCH), Electrical Engineer
PILLEUX, Mauricio (RCH), Mechanical Engineer

DEPARTURES

MIRANDA, Jorge (RCH), Night Assistant
ALVAREZ, Alberto (RCH), Night Assistant
DONOSO, Reinaldo (RCH), Mech. Maint.
CARRASCO, Marcelo (RCH), Informatics Engineer
MOLKENBUHR, Mariam (RCH), Secretary

ESO Fellowship Programme 1998/99

The European Southern Observatory (ESO) awards up to six postdoctoral fellowships tenable at the ESO Headquarters, located in Garching near Munich, and up to three postdoctoral fellowships tenable at ESO's Astronomy Centre in Santiago, Chile.

ESO facilities include the La Silla Observatory in Chile, the VLT Observatory on Cerro Paranal, and the astronomical centres in Garching and Santiago. At La Silla, ESO operates eight optical telescopes with apertures in the range from 0.9 m to 3.6 m, the 15-m SEST millimetre radio telescope, and smaller instruments. First light for the first telescope of the Very Large Telescope (VLT) consisting of four 8-m telescopes is expected in the first quarter 1998. Both the ESO Headquarters and the Astronomy Centre in Santiago offer extensive computing facilities, libraries and other infrastructure for research support. The Space Telescope European Co-ordinating Facility (ST-ECF), located in the ESO Headquarters building, offers the opportunity for collaborations. In the Munich area, several Max-Planck Institutes and the University Observatory have major programmes in astronomy and astrophysics and provide further opportunities for joint programmes. In Chile, astronomers

ESO, the European Southern Observatory, was created in 1962 to . . . establish and operate an astronomical observatory in the southern hemisphere, equipped with powerful instruments, with the aim of furthering and organising collaboration in astronomy . . . It is supported by eight countries: Belgium, Denmark, France, Germany, Italy, the Netherlands, Sweden and Switzerland. It operates the La Silla observatory in the Atacama desert, 600 km north of Santiago de Chile, at 2,400 m altitude, where fourteen optical telescopes with diameters up to 3.6 m and a 15-m submillimetre radio telescope (SEST) are now in operation. The 3.5-m New Technology Telescope (NTT) became operational in 1990, and a giant telescope (VLT = Very Large Telescope), consisting of four 8-m telescopes (equivalent aperture = 16 m) is under construction. It is being erected on Paranal, a 2,600 m high mountain in northern Chile, approximately 130 km south of Antofagasta. Eight hundred scientists make proposals each year for the use of the telescopes at La Silla. The ESO Headquarters are located in Garching, near Munich, Germany. It is the scientific, technical and administrative centre of ESO where technical development programmes are carried out to provide the La Silla observatory with the most advanced instruments. There are also extensive facilities which enable the scientists to analyse their data. In Europe ESO employs about 200 international Staff members, Fellows and Associates; at La Silla about 50 and, in addition, 150 local Staff members.

The ESO MESSENGER is published four times a year: normally in March, June, September and December. ESO also publishes Conference Proceedings, Preprints, Technical Notes and other material connected to its activities. Press Releases inform the media about particular events. For further information, contact the ESO Information Service at the following address:

EUROPEAN
SOUTHERN OBSERVATORY
Karl-Schwarzschild-Str. 2
D-85748 Garching bei München
Germany
Tel. (089) 320 06-0
Telex 5-28282-0 eo d
Telefax (089) 3202362
ips@eso.org (internet)
ESO::IPS (decnet)

The ESO Messenger:
Editor: Marie-Hélène Demoulin
Technical editor: Kurt Kjär

Printed by
Druckbetriebe Lettner KG
Georgenstr. 84
D-80799 München
Germany

from the rapidly expanding Chilean astronomical community collaborate with ESO colleagues in a growing partnership between ESO and the host country's academic community. The main areas of activity at the Headquarters and in Chile are:

- research in observational and theoretical astrophysics;
- managing and constructing the VLT;
- developing the interferometer and adaptive optics for the VLT;
- operating the La Silla Observatory;
- development of instruments for current ESO telescopes and for the VLT;
- calibration, analysis, management and archiving of data from the current ESO telescopes;
- fostering co-operation in astronomy and astrophysics within Europe and Chile.

In addition to personal research, fellows in Garching spend up to 25% of their time on the support or development activities mentioned above. These activities offer the opportunity to make short-term visits to the ESO sites in Chile and to develop in-depth knowledge of the operations of the observatory. In Chile, fellows and staff astronomers spend one week at ESO's centre in Santiago, one week at La Silla Observatory and have the third week off. At La Silla, fellows help in supporting visiting astronomers, and participate in the development and maintenance of the telescopes and instruments. The fellowship programme in Chile offers a unique opportunity to learn and to participate in the process of observational astronomy while pursuing a research programme with state-of-the-art facilities.

The basic monthly salary will be not less than DM 4853 to which is added an expatriation allowance of 9–12% in Garching, if applicable, and up to 40% in Chile. The remuneration in Chile will be adjusted according to the cost of living differential between Santiago de Chile and the lead town Munich.

The fellowships are granted for one year with the expectation of a renewal for a second year and exceptionally a third year. Fellowships begin between April and October of the year in which they are awarded. Selected fellows can join ESO only after having completed their doctorate.

Applications should be submitted to ESO not later than 15 October 1997. Applicants will be notified in December 1997 or soon thereafter. The ESO Fellowship Application Form must be used, which is available from the ESO Personnel Department or from http://www.hq.eso.org/gen-fac/adm/pers/vacant/fellow.html. The applicant should arrange for three letters of recommendation from persons familiar with his/her scientific work to be sent directly to ESO. These letters should reach ESO not later than 15 October 1997.

Further inquiries, requests for application forms, and completed applications should be addressed to:

European Southern Observatory
Fellowship Programme
Karl-Schwarzschild-Str. 2
D-85748 Garching bei München, Germany

Tel.: 0049-89-32006-438 or -219 — Fax: 0049-89-32006-497
e-mail: ksteiner@eso.org

Contents